OXFORD

Modelling the Hafnium–Neodymium Evolution of Early Earth: A Study from West Greenland

Nicholas J. Gardiner [iD] [1,2*§], **Tim E. Johnson**[1,3],
Christopher L. Kirkland[1,2§] **and Kristoffer Szilas**[4]

[1]School of Earth and Planetary Sciences, Curtin University, (§Centre for Exploration Targeting—Curtin Node), Perth, Australia; [2]Australian Research Council Centre of Excellence for Core to Crust Fluid Systems, Australia; [3]State Key Lab of Geological Processes and Mineral Resources, China University of Geosciences, Wuhan, China; [4]Department of Geosciences and Natural Resource Management, University of Copenhagen, Øster Voldgade 10, 1350 Copenhagen K, Denmark

*Corresponding author. Present address: School of Earth, Atmosphere and Environment, Monash University, Victoria 3800, Australia. Telephone: +61 (0) 3 9905 4879. Fax: +61 (0) 3 9905 4903. E-mail: nick.gardiner@monash.edu

ABSTRACT

The processes of partial melting and the segregation and migration of melt underpin the differentiation of the lithosphere. The Sm–Nd and Lu–Hf isotopic systems, which are sensitive to these processes, behave similarly during mantle–crust differentiation, leading to isotopically coupled primary (basaltic) and continental (tonalite–trondhjemite–granodiorite, TTG) crustal compositions that define a linear terrestrial fractionation array in εNd vs εHf space. However, Eoarchaean basalts and TTGs from West Greenland do not sit on this trend and are isotopically decoupled, which may reflect their extraction from a mantle with a non-chondritic composition. We explore the effects of source composition vs fractionation on the production and evolution of early Archaean crust. We use phase equilibria and trace element modelling to characterize the Hf–Nd isotopic evolution of a chain of melting from anhydrous mantle through hydrated basalt to TTG. We show that $\sim$20% decompression melting of anhydrous mantle with a superchondritic Sm/Nd but chondritic Lu/Hf composition at a mantle potential temperature appropriate to the early Archaean produces basaltic melts with an isotopic composition similar to those measured in Eoarchaean tholeiitic basalts from Isua, West Greenland. In turn, 5–30% melting of hydrated basalt produces TTG melts with Hf–Nd isotopic compositions similar to those measured in Eoarchaean TTGs from the Itsaq Gneiss Complex, West Greenland. Thus, we chart a chain of melting from an isotopically decoupled Hf–Nd mantle composition to isotopically decoupled mafic and felsic crust. Our modelling defines an overall Hf–Nd isotopic fractionation trend that is parallel to, but offset from, that defined by modern rocks with coupled compositions. Primitive mantle contamination by 5% recycled continental crust (TTG) requires a higher degree of mantle melting (30%) to produce basaltic melt with a Hf–Nd composition similar to the Isua basalts. A mantle composition with greater than 5% crustal contamination is more enriched than the Isua basalts, placing an upper limit on the amount of crustal contaminant. A non-chondritic mantle source composition in the early Archaean likely imposed a first order control on the subsequent production of crust with decoupled Hf–Nd compositions.

Key words: Archean Hadean; Itsaq Isua amphibolite; TTG tonalite gneiss; Hf Nd isotope; mantle melting anatexis

INTRODUCTION

Partial melting and the segregation and migration of melt are the fundamental processes governing the formation and differentiation of the lithosphere (e.g. Sawyer et al., 2007). One of Earth's key transformations during the Hadean to Eoarchaean (4·5–3·6 Ga) was the emergence of the first primary basaltic crust derived from partial melting of the mantle (Bennett et al., 1993; Hofmann, 1988) and the formation of a complementary residual mantle lithosphere (McKenzie & Bickle, 1988). In turn, Earth's first continental crust was produced from partial melting of hydrated basaltic crustal rocks to form felsic magmas of the tonalite–trondhjemite–granodiorite (TTG) series (Drummond & Defant, 1990; Martin, 1994; Smithies et al., 2009; Moyen, 2011; Johnson et al., 2017).

Evidence critical to understanding Earth's secular chemical evolution has been provided through both the samarium–neodymium ($^{147}Sm/^{144}Nd$) and lutetium–hafnium ($^{176}Lu/^{177}Hf$) radiogenic isotope systems (e.g. Vervoort et al., 1996; Blichert-Toft et al., 1999). These isotopic systems behave similarly during mantle–crust differentiation (Patchett & Tatsumoto, 1980). As a consequence, the majority of oceanic (i.e. basaltic) and continental (i.e. granitic *sensu lato*) crustal rocks of Phanerozoic and Proterozoic age exhibit coupled Hf–Nd compositions (Vervoort et al., 1999; Vervoort et al., 2000; Chauvel et al., 2008), in that they define a terrestrial array in εHf–εNd space (in which the isotopic compositions are normalized to chondritic values) along which the two isotopic systems co-evolve. However, oceanic and continental crustal rocks of Eoarchaean age (4·0–3·6 Ga) in West Greenland exhibit decoupled Hf–Nd compositions and plot off the terrestrial array (Vervoort et al., 2000; Caro et al., 2005; Hoffmann et al., 2011b). Such decoupling may result from the processes of partial melting, where the Lu/Hf composition of the melt is lowered due to the presence of garnet or other key phases in the residual source rocks during anataxis in the deep crust (e.g. Vervoort & Patchett, 1996; Schmitz et al., 2004; Gardiner et al., 2018). Alternatively, decoupled Hf–Nd compositions may reflect the possibility that this early Archaean crust was extracted from a mantle reservoir that itself had a non-chondritic, or decoupled, Hf–Nd (and εHf–εNd) composition (Bennett, 2003; Caro et al., 2005; Rizo et al., 2011; Hoffmann et al., 2011b).

Although the bulk composition of the Earth has commonly been assumed to be chondritic (McDonough & Sun, 1995), some workers have proposed that Earth's mantle developed a non-chondritic Sm/Nd composition during the early Hadean (Blichert-Toft et al., 1999; Boyet & Carlson, 2006; Labrosse et al., 2007; Caro & Bourdon, 2010; Rizo et al., 2011; Morino et al., 2017). The existence of a Hadean mantle with a non-chondritic Sm/Nd composition that persisted through to the early Archaean has implications for the Nd isotope composition of any crust extracted during this period.

Eoarchaean, and perhaps Hadean (O'Neil & Carlson, 2017), basalts are parents to a significant proportion of Earth's felsic continental crust, much of which was generated during the Eo- to Palaeoarchaean (Dhuime et al., 2012), and which ultimately stabilized to form the first continental nuclei (Johnson et al., 2017).

Constraining mantle melting processes, and to what extent the composition of basaltic and felsic melts reflects their mantle parentage, is important for understanding the combined Hf–Nd evolution of Earth's early mantle and crustal reservoirs. However, the primary isotopic signatures of Eoarchaean felsic crustal rocks, which potentially inform on Hadean and early Archaean mantle processes, may be obscured due to metamorphic overprinting or magma mixing (e.g. Moorbath et al., 1997). Consequently, linking the Hf–Nd composition of this early continental crust back through their basaltic parentage to a mantle composition is challenging (e.g. O'Neil & Carlson, 2017).

The Eoarchaean Itsaq Gneiss Complex of West Greenland (Nutman et al., 1996), which crops out in the Nuùk region, is one of the best exposed and most extensively studied tracts of ancient crust on Earth. It is predominantly comprised of 3·89–3·65 Ga grey orthogneisses, mostly tonalitic in composition (Nutman et al., 1999), along with spatially and temporally associated supracrustal rocks. The most notable supracrustal sequences of the Itsaq Gneiss Complex are the mafic and metasedimentary successions of the Isua Supracrustal Belt (Allaart, 1976), which include amphibolites with both tholeiitic and boninitic affinities (Polat & Hofmann, 2003; Jenner et al., 2009). Workers have deployed a variety of approaches, including trace element and isotope geochemistry, and phase equilibria modelling, to propose that the Isua tholeiites may represent the basaltic parents to the Itsaq Gneiss tonalites (Hoffmann et al., 2011b, 2014, 2019; Nagel et al., 2012).

In this contribution, we characterize the Hf–Nd evolution of a chain of melting, from initial melting of anhydrous mantle to produce primary (juvenile) basaltic crust, through partial melting of hydrated basaltic crust to produce juvenile continental (TTG) crust. Using an approach that combines thermodynamic, trace element, and isotopic, modelling, we calculate the effects of partial melting of both mantle and crust on the Hf–Nd evolution of the mantle–crust system within the context of the Eoarchaean Earth. Further, we use the approach to investigate the role of the Hf–Nd composition of the mantle source vs fractionation during partial melting, including the effects of crustal recycling, to explore the origin of decoupled Hf–Nd isotopic compositions preserved in Eoarchaean Isua basalts and TTGs from the Itsaq Gneiss Complex.

MODELLING APPROACH

Our approach to exploring the effect of partial melting of a given source (mantle or crust) on melt Hf–Nd

composition is to employ a combination of phase equi-
libria and trace element modelling.

Phase equilibria modelling

Phase equilibria modelling is a proven approach in
investigating the processes of partial melting, allowing
calculation of the composition and abundance of stable
phases (minerals, melt and volatile species), as a func-
tion of pressure, temperature and bulk composition,
assuming thermodynamic equilibrium. Here, we use
new thermodynamic solution models applicable to the
partial melting of anhydrous ultramafic rocks and
hydrated mafic rocks, to model the melting of dry man-
tle peridotite and hydrous basalt (amphibolite) respect-
ively. We calculate isochemical pressure–temperature
(*P–T*) phase diagrams, commonly termed pseudosec-
tions, using a defined major element bulk composition,
to model the composition and abundance of melt and
co-existing (residual) minerals, as a function of *P* and *T*.
Calculations used THERMOCALC version 3.45i (Powell
& Holland, 1988) and the internally consistent thermo-
dynamic data set ds63 (updated 5 Jan, 2015) of Holland
& Powell (2011) (available at: http://www.metamorph.
geo.uni-mainz.de/thermocalc/).

For mantle melting, phase equilibria modelling was
undertaken in the anhydrous eight-component chem-
ical system Na_2O–CaO–FeO–MgO–Al_2O_3–SiO_2–CrO_2–O
(NCFMASCrO) using the activity–composition (*a–X*) so-
lution models of Jennings & Holland (2015). These
models, and more recent calibrations (Holland *et al.*,
2018), currently do not permit modelling of hydrated
peridotite. Modelling basalt melting was undertaken in
the ten-component Na_2O–CaO–K_2O–FeO–MgO–Al_2O_3–
SiO_2–H_2O–TiO_2–O (NCKFMASHTO) chemical system,
which additionally allows consideration of H_2O and
K_2O. The following *a-X* were used: augite, garnet, ortho-
pyroxene, biotite, white mica, chlorite (White *et al.*,
2014); olivine, epidote (Holland & Powell, 2011); tonalit-
ic melt, augite (clinopyroxene), hornblende (amphibole)
(Green *et al.*, 2016); magnetite–spinel (White *et al.*,
2002); ilmenite–hematite (White *et al.*, 2000); C$\bar{1}$ plagio-
clase (Holland & Powell, 2003). For melting basalt, the
H_2O content in the modelled composition was fixed to
be just sufficient to saturate the solidus at 1.0 GPa (pro-
ducing <1 mol % H_2O-saturated melt). Calculations as-
sume an $Fe^{3+}/\Sigma Fe = 0.1$ (Bézos & Humler, 2005; Berry
et al., 2008).

The abundance of residual zircon during basalt melt-
ing was calculated for each melting step using the zirco-
nium (Zr) saturation calibration of Boehnke *et al.* (2013),
which derives a Zr partition coefficient given *T* and the
predicted major element composition of the melt. Using
the Zr content of the source (average Isua basalt), this
calculation predicts the Zr content of the residue, which
is then converted to weight percent zircon through div-
ision by the Zr composition of zircon (here estimated at
430 000 ppm). In all cases the mode of zircon predicted
to be in the residuum is insignificant at less than 10^{-5}%.

Table 1: Input bulk major element compositions (mol.%) used
for phase equilibria modelling. The average Isua basalt com-
position was calculated using the mean composition of nine
meta-basalt analyses (Hoffmann *et al.*, 2011b), excluding one
analysis with high K_2O and one with anomalously high Sm/Nd.
The composition of DMM is based on Workman and Hart
(2005), and for PUM on McDonough and Sun (1995).

Mol %	DMM	PUM	Isua Basalt
Na_2O	0.110	0.301	1.844
CaO	2.914	3.276	9.552
K_2O			0.177
FeO	5.928	5.850	9.679
MgO	50.000	48.963	18.437
Al_2O_3	2.036	2.274	4.746
SiO_2	38.719	39.106	48.093
TiO_2			0.618
Cr_2O_3	0.190	0.130	
O	0.100	0.100	0.481
H_2O			6.374

Melting anhydrous mantle: phase relations

We apply the phase equilibria approach to model partial
melting of both a modern depleted MORB mantle
(DMM), and a primitive upper mantle (PUM) compos-
ition, representing a depleted and undepleted dry man-
tle source, respectively. We take the DMM composition
of Workman & Hart (2005) and adopt the PUM major
element composition of McDonough & Sun (1995),
which is an estimation of the composition of the bulk
silicate Earth. Major element compositions are detailed
in Table 1.

A *P–T* pseudosection for the DMM composition in
the NCFMASCrO model system is shown in Fig. 1a. The
calculated solidus (red line) occurs at around 1700°C at
5 GPa, declining to <1200°C at pressures below 1 GPa.
Plagioclase is predicted to be stable only at *P* < 0.8 GPa
and *T* < 1200°C. Spinel (chromite) stability is restricted
to relatively low pressures (*P* < 1.5 GPa at 1000°C and <
3.3 GPa at 1700°C). At higher *P*, garnet rather than spi-
nel is stable, with the two phases coexisting over a nar-
row pressure interval (Fig. 1a). Clinopyroxene and
orthopyroxene are ubiquitous in the subsolidus region.
However, upon crossing the solidus, first clinopyroxene
(augite) and then orthopyroxene is consumed by the
melting reactions. The abundance of melt (as mol %
~vol. %), as a function of *P* and *T*, is indicated (Fig. 1a,
dashed white lines).

As a primary melt, DMM produces normal mid-ocean
ridge basalt (N-MORB), a process we model through de-
compression melting along a 0.5°C/km adiabatic geo-
thermal gradient (Fig. 1a, dashed red line, which
assumes a constant density of 3.4 gcm^{-3}), a reasonable
estimate for the upper part of the mantle (Katsura *et al.*,
2010). For modelling the modern Earth system, we as-
sume a mantle potential temperature (*T*p) of 1340°C
(Katsura *et al.*, 2010), which is here simplified as the con-
temporary mantle adiabat projected to the surface (i.e.
no conductive cooling). Along this adiabat, we track the
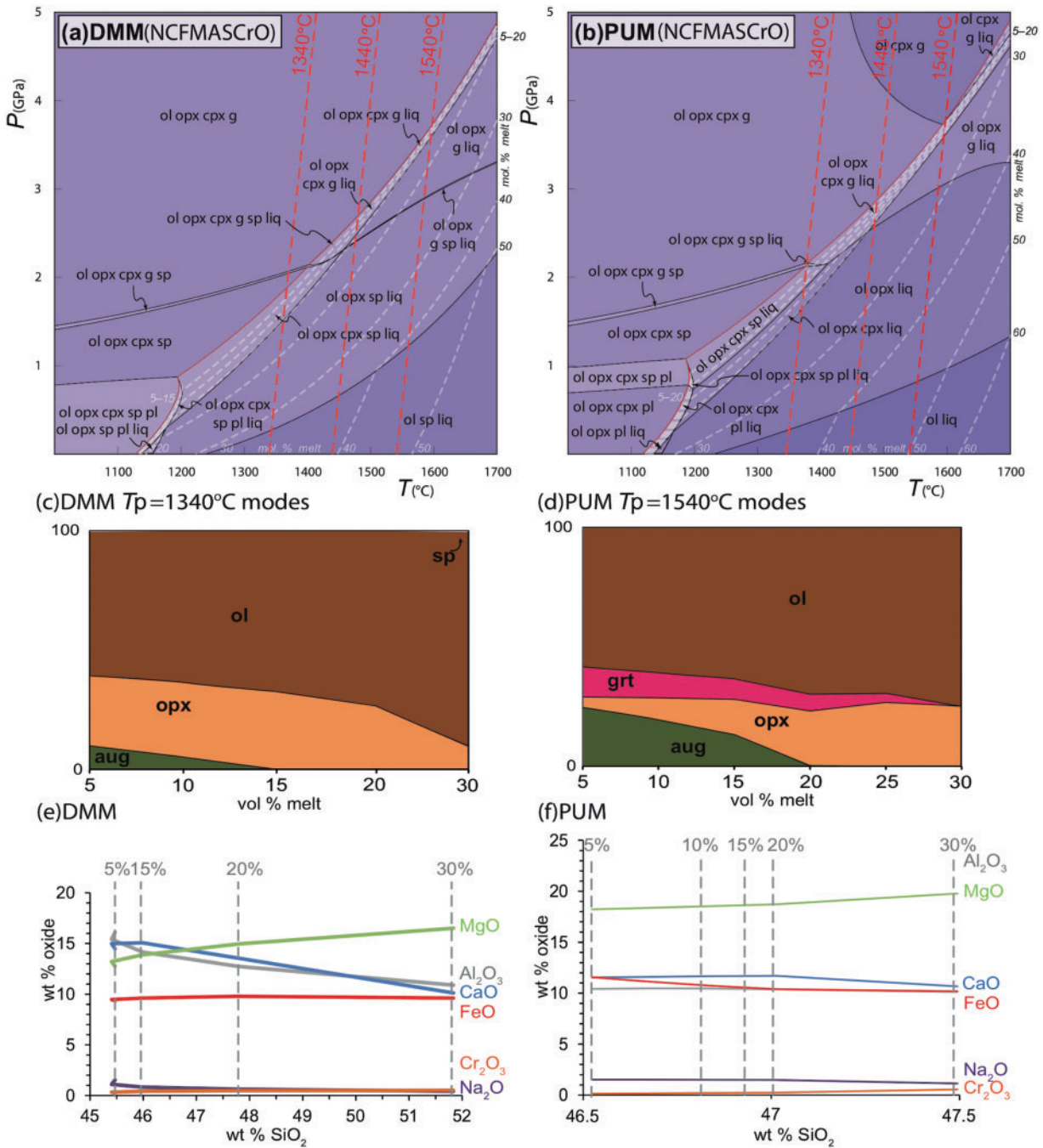
Fig. 1. Phase equilibria modelling – mantle melting. Pseudosections calculated for major element compositions of (a) depleted MORB mantle (DMM) and (b) primitive undepleted mantle (PUM). Red dashed lines represent a mantle adiabatic geothermal gradient of 0·5°C/km with mantle potential temperatures (T_p) of 1340, 1440 and 1540°C. The solid red line indicates the solidus, and melting isopleths (mol % ~ vol. %) are shown as dashed white lines. Assemblage fields are labelled with stable phases, in which abbreviations are: melt (liq), garnet (g), clinopyroxene (cpx), orthopyroxene (opx), olivine (ol), spinel (sp), plagioclase (pl). The depth of shading of assemblage fields reflects increasing variance. (c, d) Predicted residual phase modes (as mode percent, normalized to 100% excluding quartz) along the mantle adiabat for (c) DMM along a 1340°C/GPa geotherm and (d) PUM along the 1540°C/GPa geotherm. (e, f) Modelled anhydrous melt major element compositions (wt % oxide) as a function of SiO_2 and melt fraction for (e) DMM along a 1340°C/GPa geotherm and (f) PUM along a 1540°C/GPa geotherm.

progressive melting of the mantle, calculating the abundance and major element composition of both melt and residual minerals at 5, 10, 15, 20 and 30 mol % (~ vol. %) melt (see Table 2). On decompression, the onset of

melting along this adiabat is predicted to occur at around 1370°C and 1·9 GPa, within the stability field of spinel peridotite (Fig. 1a; Table 2 details the abundance of residual minerals). Figure 1c shows residual mineral

Table 2: Calculated residual phase proportions, plus melt trace element and isotopic compositions, for Depleted MORB Mantle (DMM) and the Primitive Upper Mantle (PUM) compositions by vol. % melt fraction along a mantle geotherm of 0·5°C/km assuming mantle potential temperatures of 1340, 1440 and 1540°C

P (kbar)	T (°C)	Melt Frac %	ol	sp	opx	cpx	g	Th	Nb	La	Ti	Gd	Sm	Nd	Lu	Hf	$^{147}Sm/^{144}Nd$	$^{176}Lu/^{177}Hf$
DMM Tp = 1340°C																		
18·8	1367	5	0·568	0·013	0·267	0·152	0·000	0·15	2·73	3·36	5853	4·22	2·96	8·77	0·36	1·69	0·209	0·030
17·5	1366	10	0·571	0·007	0·277	0·093	0·000	0·08	1·46	1·88	4656	3·01	2·08	5·42	0·30	1·22	0·237	0·034
16·4	1364	15	0·572	0·003	0·279	0·046	0·000	0·05	0·96	1·26	3742	2·24	1·53	3·75	0·25	0·92	0·251	0·039
15	1362	20	0·573	0·001	0·273	0·000	0·000	0·04	0·73	0·95	3095	1·73	1·17	2·86	0·22	0·73	0·252	0·042
4·7	1347	30	0·629	0·001	0·064	0·000	0·000	0·03	0·49	0·64	2288	1·18	0·79	1·92	0·17	0·51	0·254	0·048
DMM Tp = 1440°C																		
26·3	1480	5	0·574	0·000	0·221	0·096	0·059	0·15	2·74	3·40	2749	1·01	1·51	7·73	0·16	1·00	0·121	0·022
25·5	1478	10	0·567	0·000	0·256	0·040	0·033	0·07	1·38	1·79	3094	1·35	1·49	4·95	0·19	0·94	0·186	0·028
24·5	1477	15	0·562	0·000	0·274	0·000	0·014	0·05	0·98	1·28	3245	1·66	1·40	3·76	0·21	0·86	0·229	0·035
20·0	1470	20	0·561	0·002	0·239	0·000	0·000	0·04	0·74	0·97	3098	1·75	1·18	2·90	0·22	0·74	0·252	0·042
11·0	1456	30	0·586	0·004	0·111	0·000	0·000	0·03	0·50	0·64	2269	1·18	0·79	1·93	0·17	0·51	0·253	0·047
DMM Tp = 1540°C																		
36·6	1595	5	0·570	0·000	0·155	0·125	0·098	0·15	2·61	3·18	1996	0·66	1·09	6·61	0·12	0·76	0·102	0·021
36·2	1594	10	0·560	0·000	0·193	0·063	0·078	0·07	1·35	1·73	2127	0·77	1·07	4·47	0·13	0·72	0·147	0·025
35·8	1594	15	0·551	0·000	0·223	0·013	0·063	0·05	0·97	1·26	2196	0·86	1·03	3·53	0·14	0·67	0·180	0·029
32	1588	20	0·544	0·000	0·223	0·000	0·033	0·04	0·73	0·95	2389	1·08	0·99	2·79	0·16	0·64	0·219	0·035
21	1572	30	0·543	0·003	0·157	0·000	0·000	0·03	0·50	0·65	2257	1·19	0·80	1·95	0·17	0·51	0·253	0·047
PUM Tp = 1340°C																		
19·9	1370	5	0·555	0·009	0·229	0·156	0·000	1·50	12·23	10·91	9101	5·47	4·26	17·2	0·40	2·74	0·153	0·021
18·8	1368	10	0·559	0·002	0·240	0·098	0·000	0·78	6·41	6·14	7377	4·11	3·17	11·0	0·34	2·04	0·178	0·023
17·5	1366	15	0·559	0·000	0·242	0·051	0·000	0·54	4·42	4·33	6179	3·28	2·50	8·10	0·29	1·63	0·191	0·025
16	1364	20	0·559	0·000	0·238	0·002	0·000	0·39	3·25	3·22	5150	2·62	1·98	6·16	0·25	1·31	0·199	0·027
8	1352	30	0·595	0·000	0·105	0·000	0·000	0·26	2·18	2·16	3810	1·79	1·34	4·14	0·20	0·92	0·200	0·031
PUM Tp = 1440°C																		
27·8	1482	5	0·561	0·000	0·133	0·177	0·079	1·48	11·64	10·34	3757	1·17	1·98	14·0	0·15	1·46	0·088	0·015
27·2	1481	10	0·554	0·000	0·181	0·113	0·048	0·75	6·10	5·84	4361	1·57	2·07	9·80	0·19	1·45	0·131	0·018
26·5	1480	15	0·548	0·000	0·219	0·057	0·023	0·51	4·21	4·12	4814	2·04	2·06	7·54	0·22	1·39	0·168	0·022
25·7	1478	20	0·543	0·000	0·244	0·010	0·005	0·40	3·29	3·25	4943	2·42	1·94	6·18	0·24	1·28	0·194	0·026
15·5	1464	30	0·558	0·000	0·140	0·000	0·000	0·26	2·17	2·14	3753	1·78	1·33	4·12	0·20	0·91	0·200	0·030
PUM Tp = 1540°C																		
37·2	1595	5	0·556	0·000	0·039	0·235	0·116	1·42	11·12	9·53	2885	0·84	1·50	11·9	0·12	1·15	0·078	0·015
36·9	1595	10	0·547	0·000	0·081	0·175	0·094	0·76	6·12	5·72	3119	0·97	1·52	8·85	0·13	1·13	0·106	0·017
36·6	1595	15	0·537	0·000	0·125	0·112	0·072	0·52	4·24	4·09	3323	1·13	1·52	7·03	0·15	1·09	0·133	0·019
36·2	1595	20	0·529	0·000	0·170	0·047	0·053	0·39	3·24	3·21	3506	1·29	1·52	5·88	0·16	1·06	0·159	0·021
34	1591	25	0·522	0·000	0·200	0·000	0·027	0·32	2·60	2·57	3641	1·53	1·43	4·86	0·18	0·98	0·182	0·025
27	1580	30	0·521	0·000	0·175	0·000	0·000	0·26	2·16	2·13	3695	1·76	1·32	4·09	0·19	0·90	0·200	0·030

Phase abbreviations as per Fig. 1.

abundance (normalized to 100%) along the adiabat, as a function of vol. % melt. Increasing melt fraction occurs through reactions consuming mainly clinopyroxene (aug; Fig. 1c), which is exhausted at ∼1·5 GPa at melt fractions of around 15 mol % (∼vol. %). Thereafter, melt fractions increase more gradually (Fig. 1a). The first melts produced along the adiabat are silica-poor (∼45 wt % SiO₂), with high FeO content (∼9·5 wt %) (Fig. 1e). With increasing degrees of melting, FeO contents remain constant, but melt MgO content increases from ∼13 wt % to 17 wt % (Fig. 1e). At 30% melt fraction, melt SiO₂ content is ∼52 wt %.

A P–T pseudosection for the PUM bulk major element composition is shown in Fig. 1b. Calculated phase relations for PUM are broadly similar to those for DMM, although the stability fields of spinel and orthopyroxene for PUM are reduced, and the onset of melting occurs at lower T at any defined P (i.e. PUM is, as expected, more fertile). We take the same adiabatic geothermal gradient of 0·5°C/km as for melting DMM, but for the early Earth system we assume an elevated Tp of 1540°C,

appropriate for a warmer mantle (Herzberg et al., 2010) (Fig. 1b, dashed red lines). Along this warmer mantle adiabat (1540°C), the onset of partial melting of PUM is predicted to occur at ∼1600°C and 3·7 GPa, within the stability field of garnet peridotite (residual modes in Fig. 1d). Around 25 mol % (∼vol. %), melt is predicted over a small pressure range (0·1–0·2 GPa) until first clinopyroxene (at ∼3·6 GPa) and then garnet (at ∼3·0 GPa) are consumed. Melt production thereafter is more gradual. All melts of PUM along the 1540°C adiabat are silica-poor, ranging from ∼46·5 to 47·5 wt % SiO₂. Melt FeO content is slightly higher than for DMM melting (∼10·5 wt %) (Fig. 1f), and MgO higher, increasing from ∼18 wt % to ∼20 wt %.

Melting hydrous basaltic crust: phase relations

To model the processes of melting hydrous basaltic crust in the early Earth, and the production of melt of TTG composition (juvenile felsic crust), we use the average major element composition (n = 9; Table 1) of

Eoarchaean (*c.*3·8–3·7 Ga) hydrated tholeiitic metabasalts (amphibolites) from the western limb of the Isua Supracrustal Belt, Itsaq Gneiss Complex, West Greenland (Hoffmann *et al.*, 2011*b*). These compositions represent basalts whose trace element composition is thought to have been relatively unaltered by later metamorphic and/or hydrothermal processes (Polat *et al.*, 2003; Hoffmann *et al.*, 2010, 2011*b*), and which potentially represent some of the oldest extant mantle melts. Both the εHf–εNd isotopic and Hf–Nd trace element compositions, measured in these Isua basalts are non-chondritic, and in that sense are decoupled (Hoffmann *et al.*, 2011*b*). The Isua basalts are candidate source rocks to *c.*3·8–3·7 Ga Itsaq Gneiss Complex TTGs (Hoffmann *et al.*, 2019).

A *P–T* pseudosection constructed for the average Isua basalt composition is shown in Fig. 2a. We model the melting of this basaltic composition along a simplified (linear) conductive crustal geothermal gradient of 900°C/GPa (red dotted line in Fig. 2a), appropriate to infracrustal melting within thickened basaltic crust, our preferred geodynamic scenario for felsic crust production in the early Earth (Smithies *et al.*, 2009; Johnson *et al.*, 2017). Along this geothermal gradient the progressive melting of the mafic source is tracked, and the abundance and major element composition of both melt and residual minerals calculated at 5, 10, 15, 20 and 30 mol % ($\sim$ vol. %) melt, i.e. we model non-modal melting (see Table 3). The onset of melting along the 900°C/GPa geotherm is predicted to occur at around 675°C and 7·5 GPa, after which biotite is rapidly consumed, whereas hornblende is consumed more gradually with increasing *T* and melt production (Fig. 2b). Notably, along this geotherm garnet is not predicted to be stable. At low degrees of melting ($\sim$10%), the first melts, recalculated on an anhydrous weight percent basis (Fig. 2c), are silica-rich (73 wt % SiO_2), dominantly sodic ($\sim$6 wt % Na_2O) and have low K_2O ($\sim$2·5 wt %), MgO ($\sim$0·5 wt %) and FeO ($<$2 wt %). At higher degrees of melting ($\sim$20%), the silica content of the melt is lower (70 wt %), but CaO has increased from $\sim$1·5 to $\sim$2·5 wt % (Fig. 2c).

Trace element modelling

The pseudosection approach, in allowing the calculation of the composition and abundance of melt and solid (residual) phases at a given *P* and *T*, provides the framework for trace element modelling. The calculated residual stable phase assemblage in equilibrium with the melt at each discrete melting step (either along the mantle adiabat or crustal geotherm) is used to calculate bulk partition coefficients from individual published mineral–melt partition coefficients (*Kd*; Table 4). In applying the bulk *D*s [$D = \sum (Kd \cdot X)$, where *X* is the calculated mol % ($\sim$vol. %) of the mineral], to the source trace element composition in conjunction with the batch melting equation (Shaw, 1979), the Sm/Nd and Lu/Hf compositions of the melt are derived (Tables 2

and 3). These ratios are then normalized to the composition of the Primitive Mantle, PUM (McDonough & Sun, 1995) [$(Sm/Nd)/(Sm/Nd)_{PUM}$], here termed $(Sm/Nd)_N$ and $(Lu/Hf)_N$, respectively. PUM differs slightly from the mean CI chondritic reservoir (CHUR; Palme *et al.*, 2014) with values of 0·325 vs 0·360 for Sm/Nd and 0·239 vs 0·221 for Lu/Hf (PUM and CHUR respectively). Our approach allows the calculation of melt $(Sm/Nd)_N$ and $(Lu/Hf)_N$ with progressive degrees of melting of a given mantle or crust source.

### Melting paths within $(Sm/Nd)_N$ vs $(Lu/Hf)_N$ space

In our modelling we use the mineral phase relations as determined by major element phase equilibria modelling along an adiabatic or geothermal gradient to define a melting path. To explore the Hf–Nd evolution of the melt, we plot melting paths, which chart the predicted Hf–Nd melt composition for different degrees of melting, in Lu/Hf and Sm/Nd space (i.e. $(Sm/Nd)_N$ vs $(Lu/Hf)_N$) and anchoring 100% melt at the protolith Hf–Nd composition, either mantle or basalt. Figure 3 shows how this modelling works conceptually. Using a specific major element mantle composition (M1), permits calculation of the abundance and composition of stable minerals and melt at a given *P* and *T*. Modelling the melting of M1 along an adiabat, we calculate melt $(Sm/Nd)_N$ and $(Lu/Hf)_N$ for different melt fractions, defining an M1 melting path. Figure 3 demonstrates that this M1 melting path has 100% melt anchored at the PUM-normalized Hf–Nd composition of M1 (blue), or alternatively of a different mantle Hf–Nd composition M2 (orange). This allows us to track melt Hf–Nd fractionation given different mantle Hf–Nd starting compositions.

MODELLING RESULTS

DMM melting

To demonstrate the validity of our approach we model the melting of DMM to produce melt of N-MORB composition, since the average composition of both the modern mantle and N-MORB are well constrained (here, we use the compositions of Sun & McDonough (1989) and Workman & Hart (2005), respectively). The $(Sm/Nd)_N$ and $(Lu/Hf)_N$ compositions of the basaltic melt at different degrees of melting of DMM along the 1340°C mantle adiabat (Fig. 1a) are shown in Fig. 4a (black line), where they define a melting path in $(Sm/Nd)_N$ vs $(Lu/Hf)_N$ space. The trajectory of this melting path is controlled by the calculated phase relations appropriate to the major element composition of DMM for different degrees of melting of DMM. Also plotted in Fig. 4a (black square) is the $(Sm/Nd)_N$ and $(Lu/Hf)_N$ composition of N-MORB (1.511 and 0.683, respectively), calculated using the trace element composition of Sun & McDonough (1989).

The DMM melting path almost perfectly intersects the Hf–Nd composition of N-MORB (Fig. 4a) at a melt
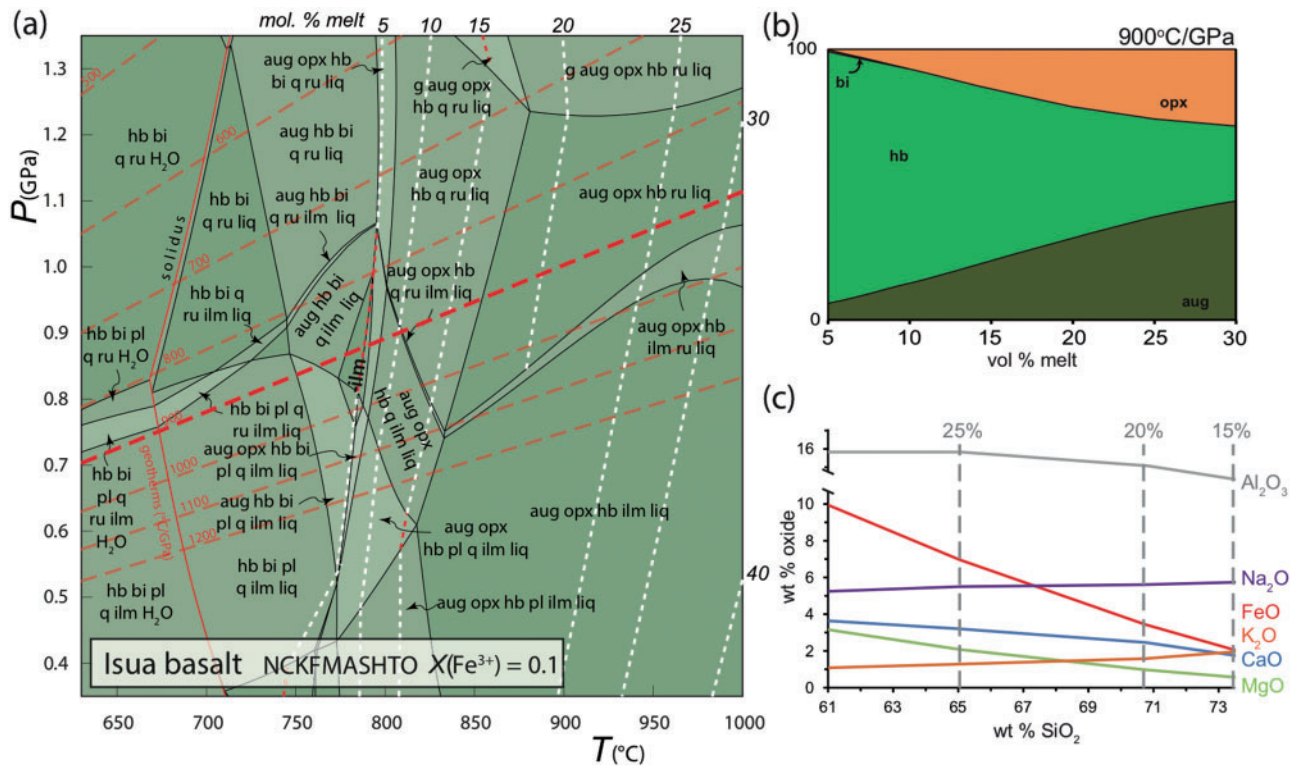
Fig. 2. Phase equilibria modelling – Isua basalt melting. (a) Pseudosection calculated for the major element composition of the average Isua basalt (n = 9). Red dashed lines represent different geothermal gradients; the 900°C/GPa geotherm along which melting is modelled is highlighted in bold. Melting isopleths (mol % ~ vol.%) are shown as dashed white lines. Assemblage fields are labelled with stable phases, in which abbreviations are: melt (liq), garnet (g), clinopyroxene (aug), orthopyroxene (opx), hornblende (hb), biotite (bi), plagioclase (pl), ilmenite (ilm), quartz (q), rutile (ru) and aqueous fluid (H_2O). The depth of shading of assemblage fields denotes increasing variance. (b) Predicted residual phase modes (as mode percent, normalized to 100% excluding quartz) along a 900°C/GPa geotherm. Quartz is excluded as it is considered to be in excess. (c) Modelled anhydrous melt major element compositions (wt % oxide) as a function of SiO_2 and melt fraction along the 900°C/GPa geotherm, normalized excluding H_2O.

Table 3: Calculated residual phase proportions, plus melt isotopic compositions, for the Isua basalt composition by vol. % melt fraction along the 700 and 900°C/GPa geotherms

T (C)	Melt Frac %	cpx	aug	pl	hb	bt	g	ilm	zrc	$^{147}Sm/^{144}Nd$	$^{176}Lu/^{177}Hf$
700°C/GPa											
798	5	0·086	0·007	0·000	0·806	0·005	0·000	0·000	0·00000	0·111	0·006
820	10	0·159	0·081	0·000	0·627	0·000	0·000	0·000	0·00000	0·114	0·007
855	15	0·225	0·139	0·000	0·470	0·000	0·000	0·000	0·00000	0·118	0·008
901	20	0·282	0·171	0·000	0·316	0·000	0·028	0·000	0·00000	0·119	0·009
966	25	0·331	0·172	0·000	0·172	0·000	0·072	0·000	0·00000	0·119	0·010
1014	30	0·355	0·161	0·000	0·087	0·000	0·091	0·000	0·00000	0·122	0·012
900°C/GPa											
788	5	0·055	0·000	0·000	0·842	0·007	0·000	0·000	0·00000	0·111	0·006
808	10	0·118	0·063	0·000	0·689	0·000	0·000	0·007	0·00000	0·114	0·006
836	15	0·183	0·122	0·000	0·531	0·000	0·000	0·006	0·00000	0·117	0·007
887	20	0·242	0·169	0·000	0·387	0·000	0·000	0·008	0·00000	0·122	0·009
950	25	0·285	0·192	0·000	0·270	0·000	0·000	0·008	0·00000	0·128	0·010
992	30	0·309	0·197	0·000	0·191	0·000	0·000	0·007	0·00000	0·135	0·012

Phase abbreviations as per Fig. 2.

fraction of ~7%. We model batch melting, and for this scenario a melt fraction of 7% is consistent with, or slightly less than, other estimates of the effective aggregate mantle melting required to produce the composition of present-day oceanic crust (e.g. Hofmann, 1988; Plank *et al.*, 1995; Workman & Hart, 2005; Herzberg & Rudnick, 2012). The N-MORB Hf–Nd composition of

Sun & McDonough (1989) is similar to that of Hofmann (1988), but plots at lower $(Sm/Nd)_N$ and $(Lu/Hf)_N$ (1·51 and 0·68, respectively), closer to ~5% on the DMM melting curve. Interestingly, these results show that, even at low degrees of melting, the Hf–Nd composition of the melt is decoupled, in that it lies off the chondritic array. In summary, our modelling reproduces Hf–Nd trace

element fractionation during melting of DMM to pro-
duce melts of the composition of N-MORB at a melt
fraction that is consistent with independent estimates.

Eoarchaean mantle melting arrays
Composition of an Eoarchaean mantle reservoir
To explore how the Hf–Nd composition of Eoarchaean
tholeiitic basalts, such as those at Isua, relates to that of
the mantle from which they were extracted, requires
reasonable constraints on both (a) the major element
and (b) the Lu/Hf and Sm/Nd compositions of a mod-
elled Eoarchaean mantle reservoir. We take the major
element compositions of DMM (depleted mantle) and

Table 4: Mineral–melt partition coefficients used, appropriate
for the anatexis of mafic and ultramafic rocks

phase	Cpx	aug	ol	sp	g	hb	bt	ilm
Kds								
Nd	0·115	0·0028	0·003[3]	0·240[4]	0·222	1·2[6]	0·03	0·01
Sm	0·259	0·0085	0·004[3]	0·180[4]	1·43	2·0[6]	0·04	0·009
Hf	0·233[1]	0·06[2]	0·009[3]	0·003[4]	1·25[5]	0·54[6]	0·023	0·38
Lu	0·28[1]	0·22[2]	0·053[3]	0·001[4]	3·79[5]	2·1[6]	0·12	0·084
Th	0·0062	0·0015	0·0009	0·001	0·0075			
Nb	0·0045	0·0058	0·0008	0·01	0·04			
La	0·052	0·0012	0·0002	0·0006	0·028			
Ti	0·288	0·1405	0·0132	0·125	2·63			
Gd	0·276	0·0215	0·005	0·0006	4·84			

All follow Bédard (2006), apart from: (1) McKenzie & O'Nions
(1991); (2) Irving & Frey (1976); (3) Kennedy *et al.* (1993); (4)
Elkins *et al.* (2008); (5) Harui *et al.* (1994); (6) Bacon & Druitt
(1988). Phase abbreviations as in Figs 1 and 2.

PUM (primitive mantle) as bracketing compositions,
supposing that a depleted Eoarchaean mantle compos-
ition must lie somewhere between them. Since the
Archaean mantle was on average hotter than on mod-
ern Earth (Herzberg *et al.*, 2010), we model the melting
of the DMM and PUM reservoirs along the same adia-
batic thermal gradient as before (0·5°C/km), but with an
elevated *T*p (1540°C), that is 200°C warmer than at pre-
sent (Katsura *et al.*, 2010). These calculations yield melt-
ing paths for DMM and PUM in (Sm/Nd)$_N$ vs (Lu/Hf)$_N$
space, which together bracket an Eoarchaean mantle
melting array (plotted in Fig. 4b in grey, anchored at the
Hf–Nd composition of PUM). This melting array defines
the range of possible melt Hf–Nd compositions result-
ing from melting a modelled Eoarchaean mantle at an
elevated *T*p. The average (Sm/Nd)$_N$ and (Lu/Hf)$_N$ com-
position of the Isua basalts is also plotted in Fig. 4b (red
square), which lies at super-chondritic (Sm/Nd)$_N$ and
sub-chondritic (Lu/Hf)$_N$ values (1·241 and 0·444, respect-
ively). The Eoarchaean mantle melting array anchored
at PUM does not intercept the Isua basalts, with the im-
plication that, within our modelling constraints, the Hf–
Nd composition of the Isua basalts cannot be attained
from directly melting a mantle of PUM Hf–Nd composi-
tion at any degree of melting (Fig. 4b).

For a modelled Eoarchaean mantle Hf–Nd compos-
ition we take a super-chondritic Sm/Nd of ∼0·360 ((Sm/
Nd)$_N$ = 1·434; ^{147}Sm/^{144}Nd ∼0·221) (Rizo *et al.*, 2011)
and Lu/Hf equal to that of PUM (red diamond; Fig. 4b).
Anchoring the Eoarchaean mantle melting array at this
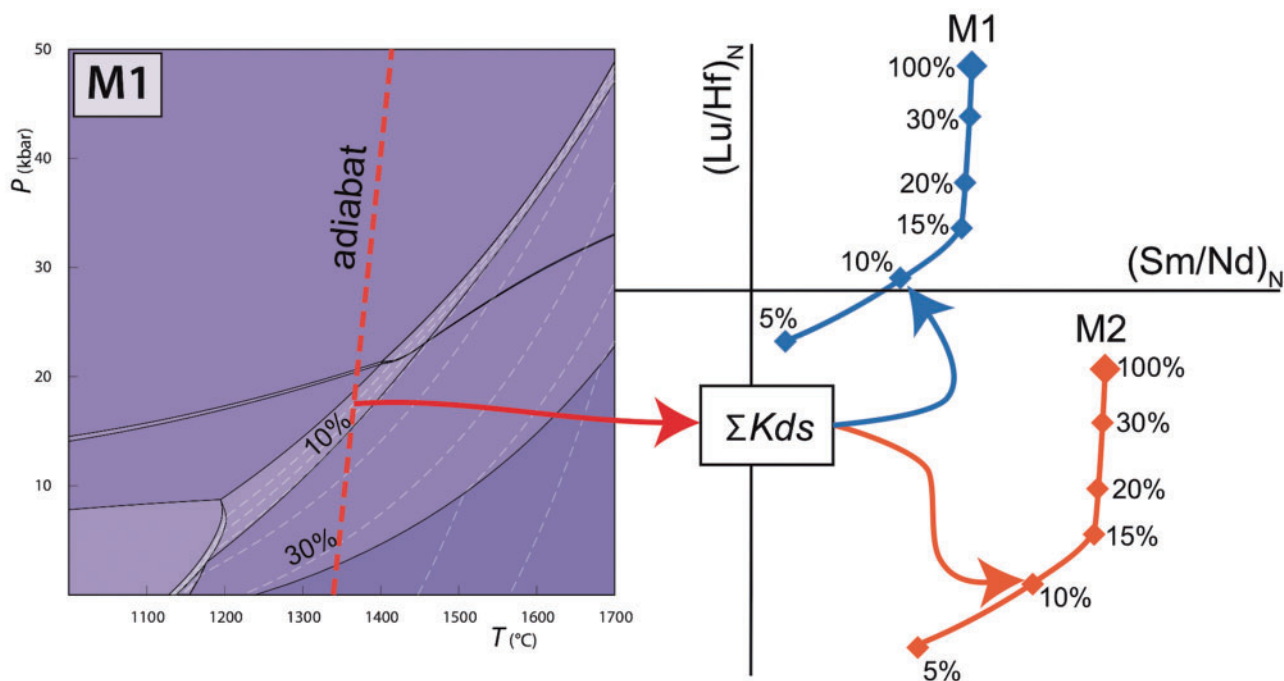
Fig. 3. Cartoon showing the conceptual link between the phase equilibria modelling, based on major element composition, and
trace element modelling, which together define melting paths in PUM-normalized (Sm/Nd)$_N$ vs (Lu/Hf)$_N$ space. Melting paths are
the calculated PUM-normalized Hf–Nd composition of the melt for different degrees of melting (annotated, %), and where 100%
melt is anchored at the Hf–Nd composition of its protolith (e.g. M1 or M2).
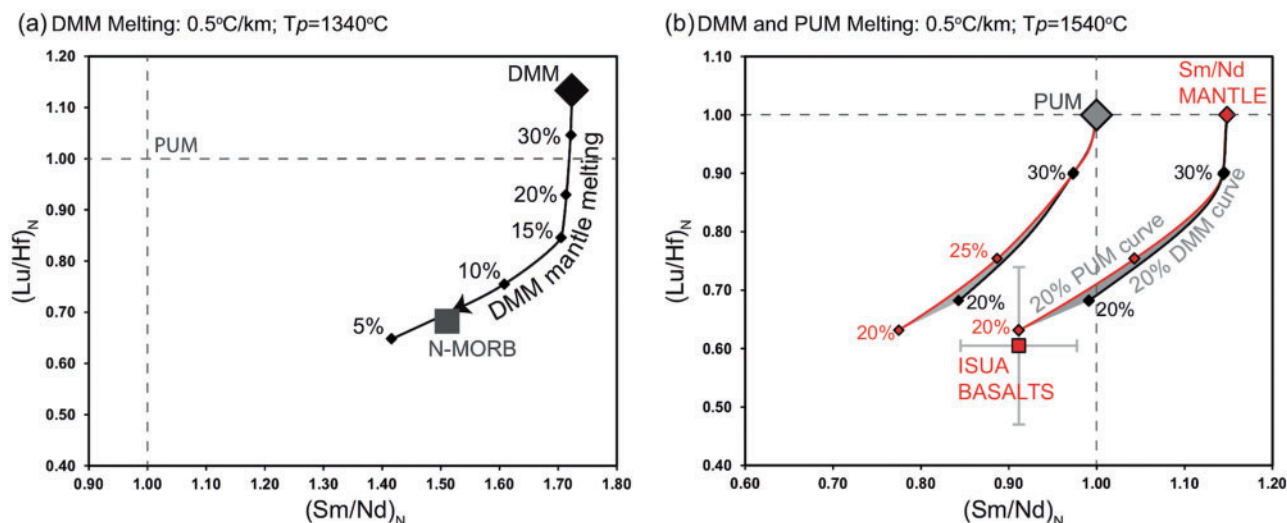
Fig. 4. Mantle melt modelling, Sm/Nd and Lu/Hf evolution. (a) The modern Earth system, melting depleted MORB mantle (DMM). Axes are calculated Lu/Hf and Sm/Nd compositions normalized to PUM. Decompression melting of DMM along a 0·5°C/km mantle adiabat with a mantle potential temperature of 1340°C defines a melting path (black line). A ~7% melt has a $(Sm/Nd)_N$ and $(Lu/Hf)_N$ composition close to modern normal mid-ocean ridge basalt (N-MORB). (b) The Eoarchaean Earth System. The PUM and DMM melting curves define an Eoarchaean melting path, this is shown anchored at the Hf–Nd composition of both PUM and that of a super-chondritic Sm/Nd mantle. Also plotted is the average Isua basalt $(Sm/Nd)_N$ and $(Lu/Hf)_N$ composition (indicated uncertainty 1σ).

mantle composition, we show that ~20% melting of a PUM-like mantle at a Tp of 1540°C, yields basaltic melts which are a good fit for the Hf–Nd composition of the Isua basalts.

$^{176}Lu/^{177}Hf$ and $^{147}Sm/^{144}Nd$ decoupling

The calculated melt Lu/Hf and Sm/Nd can be converted to an isotopic composition ($^{176}Lu/^{177}Hf$ and $^{147}Sm/^{144}Nd$) using atomic abundances and weights (Appendix). These parental isotopic ratios determine the temporal ingrowth of radiogenic ^{176}Hf and ^{143}Nd, thus the development of $^{176}Hf/^{177}Hf$ and $^{143}Nd/^{144}Nd$ (εHf and εNd), respectively.

The coupling state of $^{176}Lu/^{177}Hf$ and $^{147}Sm/^{144}Nd$ is assessed through adopting the isotopic fractionation notation of Vervoort *et al.* (2000). The fractionation of the melt isotopic composition away from that of the present-day chondritic reservoir (CHUR) of Bouvier *et al.* (2008), is calculated as $[((^{176}Lu/^{177}Hf)/(^{176}Lu/^{177}Hf)_{CHUR})-1]$, and similarly for $^{147}Sm/^{144}Nd$, termed $f(^{176}Lu/^{177}Hf)$ and $f(^{147}Sm/^{144}Nd)$ for the respective parent-daughter isotope ratios. The estimate of CHUR is the best approximation of the isotopic composition of the bulk silicate earth, i.e. PUM. If $F = f(^{176}Lu/^{177}Hf)/f(^{147}Sm/^{144}Nd)$, then $F = 1\cdot5$ is taken to imply that the modelled isotopic systems are coupled and will evolve to lie on the terrestrial fractionation array. Deviation from this slope implies a decoupled composition, resulting in the progressive separation of the two isotopic systems with time from the terrestrial array.

Our aim is to investigate whether the decoupled Hf–Nd composition of Eoarchaean felsic (TTG) crust from the Itsaq Gneiss Complex of West Greenland may reflect a decoupled composition of the Eoarchaean

mantle reservoir from which it was ultimately extracted. We model an evolutionary chain of melting from mantle, through basalt, to TTG, taking a super-chondritic Sm/Nd (decoupled) mantle composition as a starting point. For simplicity, we assume a single mantle melting event to produce the Isua basalts, and then a single basalt melting event to produce TTG. From the modelled mantle composition is projected the Eoarchaean mantle melting array (grey shading). Assuming 20% mantle melting to generate Eoarchaean basaltic (primary) crust, this array defines two end-member (basalt) melt compositions at X and X', 20% melts of PUM and DMM, respectively. These two points, X and X', are in turn taken as starting Hf–Nd compositions for modelling basalt melting. Anchoring the melting path for the average Isua basalt, calculated along the 900°C/GPa geotherm at both X and X', defines a melting array for the Isua basalts, in a manner similar to that described for Eoarchaean mantle melting. We use this basalt melting array to calculate the range of Hf–Nd isotopic compositions of TTG melts for 5 to 30% basalt melting. This evolutionary chain of melting is shown in Fig. 5.

The Isua basalts, whose Hf–Nd composition is a good fit for 20% melting of a super-chondritic Sm/Nd mantle reservoir (Fig. 5), record a decoupling of Hf and Nd (Hoffmann *et al.*, 2011*b*). In turn, projecting the Isua basalt melting array from the mantle melting array yields melts which are also decoupled (black triangles and green diamonds; Fig. 5). These melts are of TTG composition, and their Hf–Nd isotopic compositions plot close to data reported from Itsaq Gneiss Complex TTGs (Fig. 5), especially at low degrees of melting, which is feasible (Zhu *et al.*, 2011).
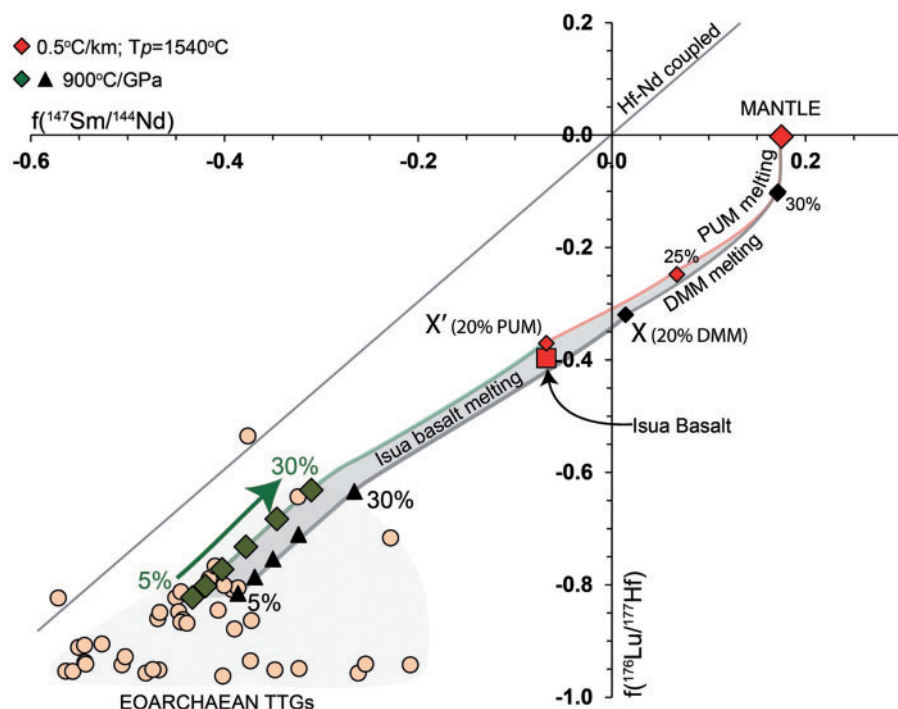
Fig. 5. Hf–Nd isotopic evolution from Eoarchaean mantle through basalt to TTG melt. Axes are calculated [147]Sm/[144]Nd and [176]Lu/[177]Hf isotopic compositions normalized to CHUR of Bouvier *et al.* (2008). Compositions which are coupled with respect to Sm/Nd and Lu/Hf lie on the 'Hf–Nd coupled' line. We model 20% decompression melting of DMM and PUM from a mantle of a super-chondritic Sm/Nd (Sm/Nd ∼0·360), and PUM Lu/Hf composition, along a 0·5°C/km adiabat with *T*p of 1540°C. This yields melt products with an [147]Sm/[144]Nd isotopic composition similar to the average of the Isua basalts (red square). Melt modelling of the Isua basalt major element composition along the 900°C/GPa geothermal gradient at 5–20% melting in turn yields TTG melts with a decoupled isotopic composition. Plotted isotopic compositions of Eoarchaean TTGs from the Itsaq Gneiss Complex, West Greenland (orange circles) are either calculated from reported trace element compositions (Nutman *et al.*, 2007; Hoffmann *et al.*, 2011a) or reported isotopic compositions (Vervoort *et al.*, 1996).

DISCUSSION

### Modelling inputs and approach

Eoarchaean mantle composition

Deciphering the composition of Earth's early mantle is challenging, especially as there is an almost complete lack of geological evidence in the form of Hadean crustal rocks. However, the Lu/Hf and Sm/Nd composition of an Eoarchaean mantle parent to the Isua metabasalts is reasonably well constrained. Sm–Nd whole-rock isochrons measured in Eoarchaean metabasalts from Isua have initial [143]Nd/[144]Nd ratios above that of CHUR (Caro *et al.*, 2005; Rizo *et al.*, 2011; Rizo *et al.*, 2013). These compositions are interpreted as representing depletion of the mantle in Nd, consistent with the positive [142]Nd anomalies (μ[142]Nd) of up to 20 ppm relative to the terrestrial standard, also measured in Isua metabasalts (Boyet *et al.*, 2003; Caro *et al.*, 2006; Rizo *et al.*, 2011). Unlike the [143]Nd record, [142]Nd anomalies are not expected to be affected by subsequent alteration of samples. These lines of evidence imply the mantle source to the Eoarchaean Isua basalts was a reservoir of super-chondritic Sm/Nd composition (i.e. an original excess of [146, 147]Sm).

For an Eoarchaean mantle composition, we assume non-chondritic Sm/Nd and chondritic Lu/Hf. Chronometry of the Eoarchaean Isua basalts using the combined [146, 147]Sm–[142, 143]Nd system has been used to calculate the composition and timing of early Hadean mantle differentiation. These measurements have yielded [147]Sm/[144]Nd compositions of between 0·219–0·226 (Sm/Nd between 0·355–0·366), with a minimum age of differentiation between 4·53 and 4·32 Ga, depending on the model chosen (Caro *et al.*, 2005; Rizo *et al.*, 2011; Morino *et al.*, 2017). In addition, zircon Hf isotope data from the Itsaq Gneiss Complex supports a chondritic Lu/Hf mantle reservoir in the Eoarchaean, at least up until 3·8 Ga (Hiess & Bennett, 2016; Fisher & Vervoort, 2018), and chondritic εHf values have been measured in the Isua tholeiitic basalts (Hiess *et al.*, 2009; Hoffmann *et al.*, 2011b; Næraa *et al.*, 2012). An upper mantle that differentiated to be super-chondritic with respect to Sm/Nd, but was chondritic for Lu/Hf is, by definition, decoupled.

The lower mantle phase Ca-perovskite uniquely fractionates Sm/Nd, but not Lu/Hf (e.g. Rizo *et al.*, 2011). Consequently, a super-chondritic Sm/Nd upper mantle composition in the Eoarchaean may reflect an early Hadean depletion event due to development of a terrestrial magma ocean and the accompanying crystallization of Ca-perovskite (e.g. Caro *et al.*, 2005; Corgne *et al.*, 2005; Liebske *et al.*, 2005; Jackson *et al.*, 2014). Defining the major element composition of a depleted
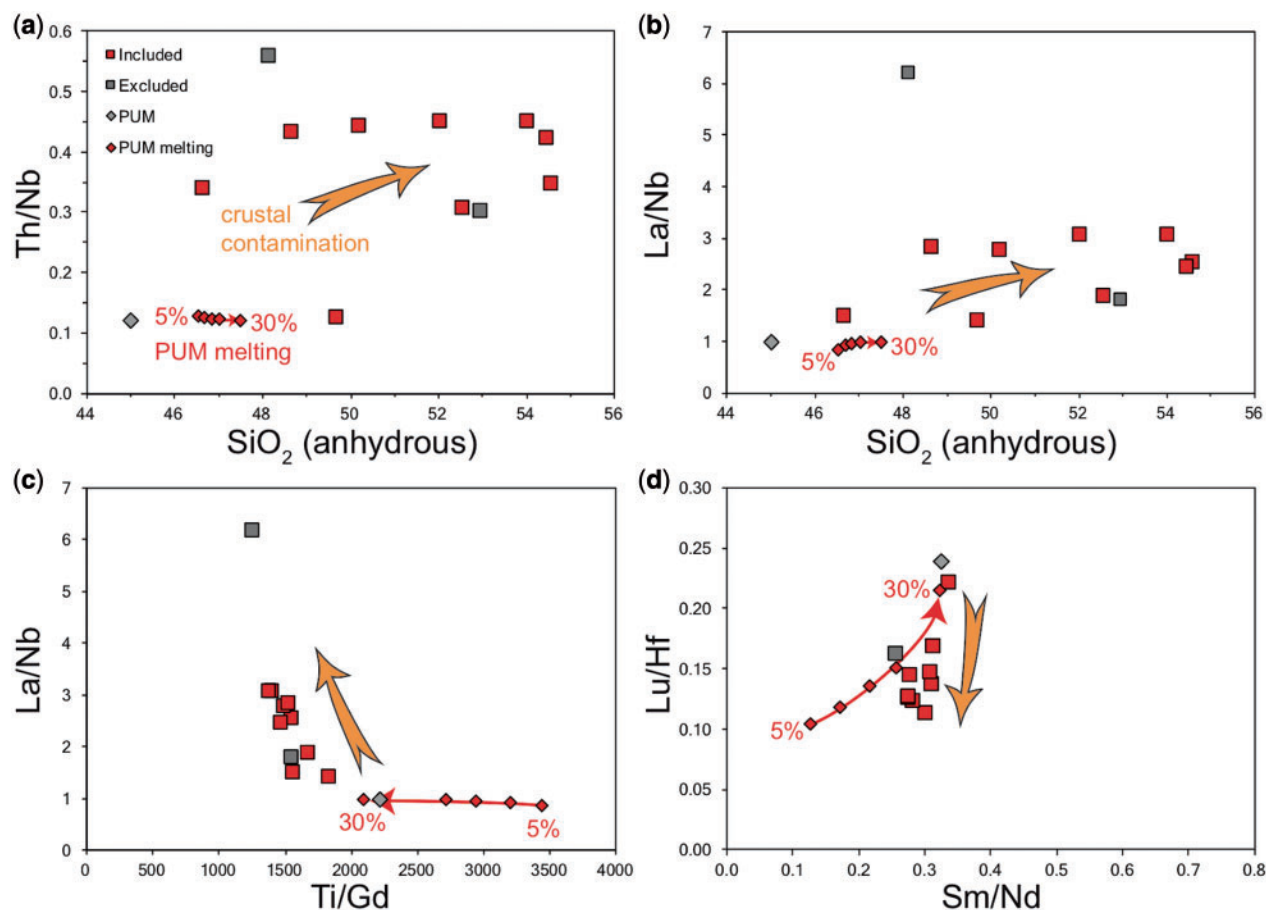
Fig. 6. Variation diagrams for samples of the Isua metabasalts of Hoffmann *et al.* (2011*b*). (a) Th/Nb vs wt % silica (SiO₂ anhydrous) concentrations; (b) La/Nb vs wt % SiO₂; (c) La/Nb vs Ti/Gd; (d) Lu/Hf vs Sm/Nd. Isua basalt analyses included in the average values used in modelling are shown as red squares, the two excluded analyses are shown as grey squares. The composition of PUM is marked (grey diamond), as is the PUM melting curve from 5–30% melting (red diamonds). The orange arrows illustrate the effects of crustal contamination.

upper mantle arising from this process is outside the scope of this contribution. Nonetheless, it is reasonable that the major element composition of an Eoarchaean upper mantle is likely to be bracketed by the compositions of (a) depleted N-MORB mantle (DMM) and (b) primitive upper mantle (PUM) as a proxy for the bulk silicate Earth. Since the major element composition of PUM taken here differs only slightly to that of DMM, both have similar melting paths in f(Sm/Nd) vs f(Lu/Hf) space (*viz.* Fig. 4b).

Isua basalt composition

Geochemical analyses of the Isua basalts were chosen based on a survey of the existing data for Isua tholeiitic basalts (e.g. Polat *et al.*, 2003; Jenner *et al.*, 2009; Hoffmann *et al.*, 2011*b*). Of these data, only Hoffmann *et al.* (2011*b*) provide independent isotope dilution data for Sm, Nd, Lu and Hf, which are the key trace elements for the present study. Rejection of two obvious outliers, one with elevated K₂O and another with anomalously high Sm/Nd (grey squares; Fig. 6), from the data of Hoffmann *et al.* (2011b), resulted in the average values used in our modelling (Table 1). The 2σ uncertainties on

our average Isua basalt composition are ∼0·04 (Sm/Nd), and ∼0·06 (Lu/Hf). An evaluation of these selected samples in comparison to the total available Isua tholeiitic basalt dataset outlined above reveals no discernible difference between their average compositions. Furthermore, our selected average Isua basalt plots along the fractional crystallization trend for the tholeiitic rocks at Isua calculated by Szilas *et al.* (2015). Thus, we suggest that the selected average composition used in the present study represents a reasonable estimate of the integrated composition of Eoarchaean mafic crust.

The magmatic parents of the Isua basalts likely experienced crystal fractionation. However, the effects of crystal fractionation are negligible with respect to their Hf–Nd systematics, because: (a) olivine dominated the fractional crystallization evolution of the Isua basalts (Szilas *et al.*, 2015), in which none of the trace elements of interest are compatible; (b) no relevant (e.g. La/Sm, Hf/Lu, Nd/Sm) trace element ratios show any co-variance with MgO or other parameters that would otherwise imply assimilation during fractional crystallization (Hoffmann *et al.*, 2011*b*); and (c) although anomalies in Sr and Eu imply late fractionation (either
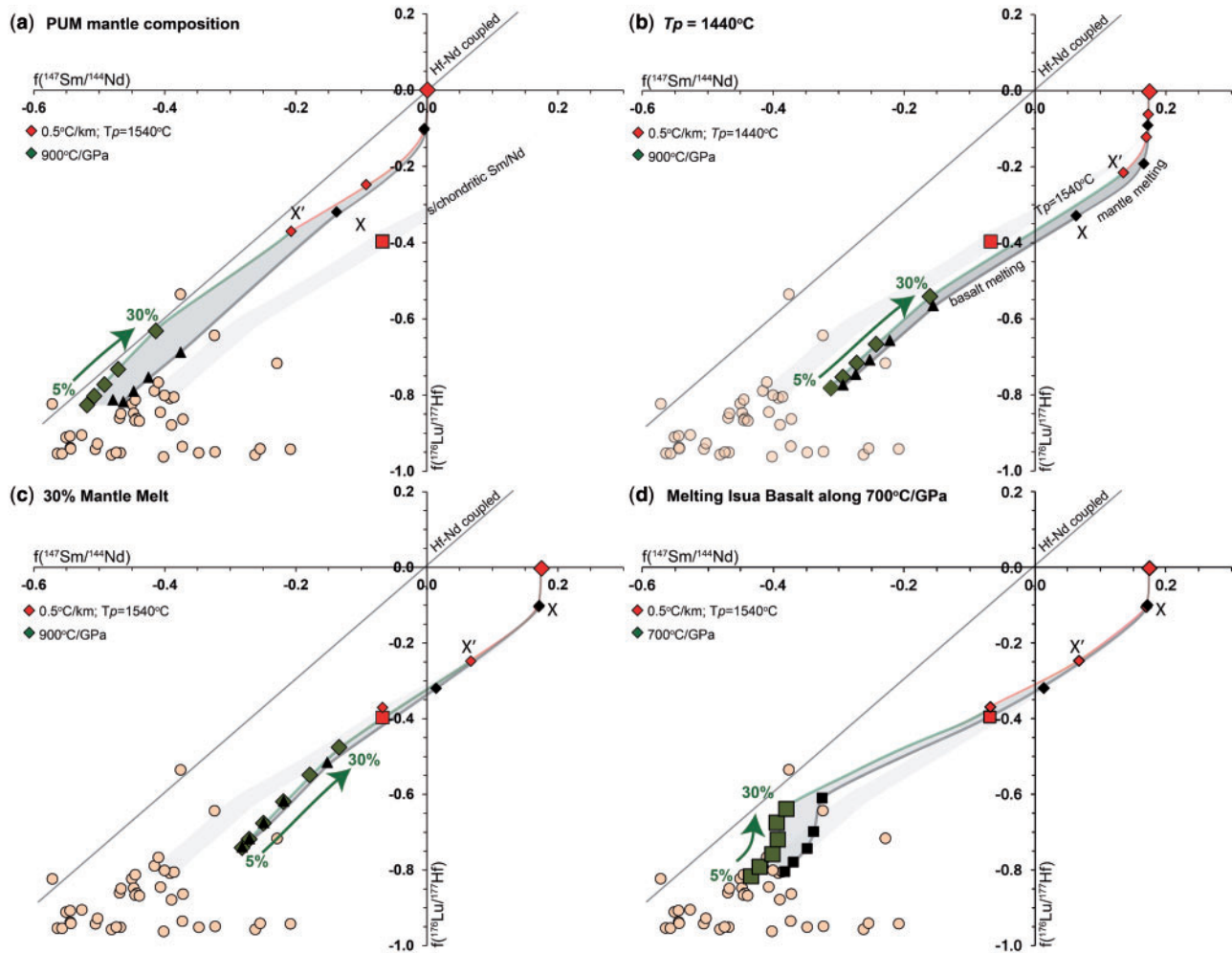
Fig. 7. Exploring the effects of: (a) chondritic Sm/Nd starting mantle composition; (b) lower Tp of 1440°C; (c) higher degree (30%) of mantle melting; (d) melting the Isua basalt along a 700°C/GPa geotherm on the overall Hf–Nd fractionation from mantle to TTG.

loss or accumulation) of plagioclase (Szilas *et al.*, 2015), this has no effect on the Hf–Nd composition of the evolved melts.

Mantle modelling sensitivities

To explore the effects of varying the modelling inputs: starting mantle composition, mantle potential temperature, and degree of mantle melting, models were run where these inputs are independently modified, and results are shown in Fig. 7. A chondritic starting mantle composition (Fig. 7a) has the effect of shifting the array towards more enriched Sm/Nd compositions, as would be expected given the starting composition is itself more enriched. The resulting TTG melt is closer to having a coupled Hf–Nd composition than that with the non-chondritic mantle, especially that derived from PUM melting.

The choice of Tp affects the stability and modes of phases during adiabatic mantle melting. Comparing the mantle adiabat anchored at a Tp of 1440 vs 1540°C (Fig. 1) shows that for DMM and PUM melting, garnet is

exhausted by 20% mantle melting at the lower Tp, while for the higher Tp, garnet is stable until at least 25% mantle melting. Plotting the melting arrays for the lower Tp, shows that the net effect is to shift both basaltic and TTG melts towards less enriched Sm/Nd compositions (Fig. 7b).

A further control on the overall Hf–Nd fractionation from mantle to TTG, is the degree of mantle melting chosen. The curvature of the melting array in Hf–Nd space implies that below 25% mantle melting, the melting path has more impact on the overall fractionation of Sm/Nd than Lu/Hf (Fig. 7c). In comparison, the degree of basalt melting taken is of less importance, as the predicted Hf–Nd fractionations from reasonable melt fractions (5–30%) are small, and the Hf–Nd compositions of resultant TTG melts are similar.

We model anhydrous mantle melting. Clearly, the presence of small quantities of H_2O in the mantle source rocks will lower the solidus temperature and produce more melt at any specified (supra-solidus) P and T, with potential consequences for the stability of
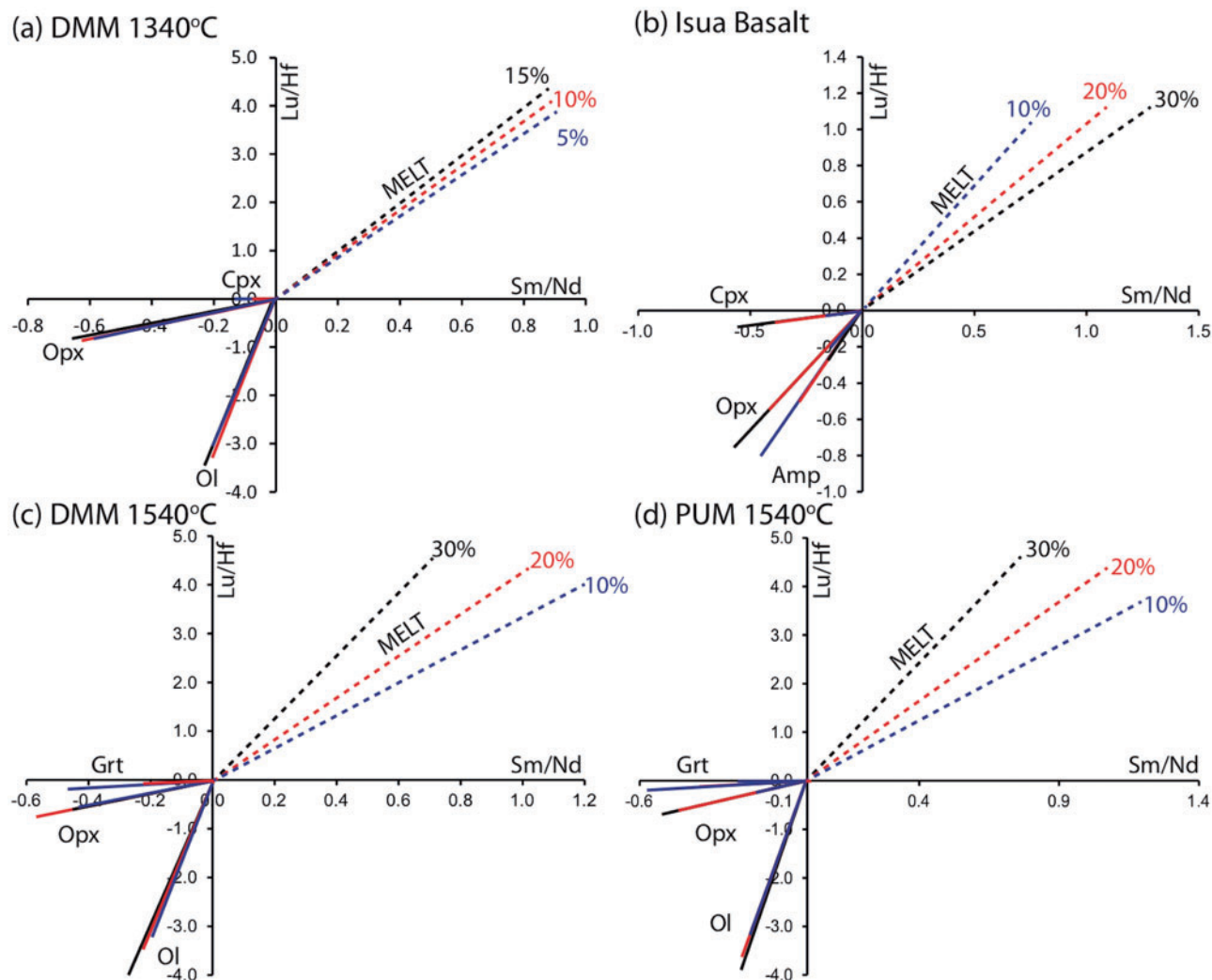
Fig. 8. Phase control on the Hf–Nd melt composition as a function of melt fraction for (a) DMM with Tp at 1340°C; (b) the Isua Basalts along the 900°C/GPa geotherm; and (c) DMM and (d) PUM with Tp of 1540°C. Axes are $[(Kd^{Sm}_p/Kd^{Nd}_p)-1*X_p]$ and $((Kd^{Lu}_p/Kd^{Hf}_p)-1*X_p]$, i.e. the ratio of Kds for mineral phase p. The arrows thus represent phase control vectors in Hf–Nd space, with negative values representing enrichment in the denominator element. The melt vectors (dotted lines) are an aggregate of the mineral phase vectors for each melt fraction, which determines the overall calculated Hf–Nd composition of the melt.

the silicate minerals. However, it is currently not possible to quantitatively model these effects, which awaits further development of appropriate solution models.

Phase control on Hf–Nd compositions

The plots in Fig. 8 detail residual mineral control on melt Hf–Nd composition as a function of melt fraction, for DMM with a Tp of 1340°C (Fig. 8a) and DMM and PUM at 1540°C (Figs 8c and d), and for the Isua basalts (Fig. 8b). The axes represent the normalized ratio of mineral/melt Kds multiplied by the calculated abundance of the mineral at each melt fraction; the ensuing composition of melt is also shown (dotted lines). Taking olivine as an example, the value on the x-axis (Sm/Nd sensitivity) is calculated as $[-(Kd^{Sm}_{Ol}/Kd^{Nd}_{Ol})-1*X_{ol}]$, where X_{ol} is the weight fraction of olivine. The lines, therefore, represent vectors in Hf–Nd space, with negative values representing (mineral) enrichment in Nd

and/or Hf. The melt vector (dotted lines, Fig. 8) is an aggregate of the phase vectors, which determines the overall calculated Hf–Nd composition of the melt; these are positive values, and thus show melt enrichment in the incompatible elements Sm and Lu.

In melting DMM given a Tp of 1340°C (i.e. modern Earth; Fig. 8a), at all melt fractions from 5–20%, olivine is the principal control on melt Lu/Hf fractionation, whilst orthopyroxene is the primary control on melt Sm/Nd fractionation. In comparison, garnet and clinopyroxene exert minimal control, in part due to their low modes during melting. Interestingly, for most melt fractions the mineral phase control on melt Hf–Nd fractionation is similar, however clinopyroxene is only stable between 5 and 10% DMM melting, and its loss by 15% mantle melting causes the observed kink in the trajectory of the melting path in Fig. 3a. The same plot for the Isua basalts is shown in Fig. 8b, which shows that both orthopyroxene and amphibole dominate both Lu/Hf and

Sm/Nd fractionation, with a minor contribution from clinopyroxene to Sm/Nd fractionation, mainly at 30% melting.

Figure 8c and d show the same plots for DMM and PUM for melting along an adiabat with a Tp of 1540°C. Again, olivine and orthopyroxene (where present) are the major controls on Lu/Hf and Sm/Nd fractionation, respectively. We find that garnet, where present, has a greater control on melt Sm/Nd fractionation than Lu/Hf.

Phase equilibria and trace element modelling inherently contains a number of assumptions, including that thermodynamic equilibrium was attained, and that use of the batch melting equation is appropriate. We choose partition coefficients (Kd) which are appropriate to melting of mafic and ultramafic rocks (Table 4).

Hf–Nd evolution from mantle to TTG

We seek to better constrain the roles of mantle source composition vs the effects of partial melting on the Hf–Nd compositions of Eoarchaean basalts and TTGs. Our modelling of decompression melting of DMM reproduces well the composition of N-MORB at appropriate melt fractions. In the early Earth scenario, the modelling yields a melting array that provides a reasonable fit for the measured Hf–Nd compositions of both the Isua tholeiitic basalts and TTGs for appropriate degrees of melting of the mantle (20%), and of basalt (5–30%), respectively (Fig. 5).

This evolutionary chain of melting charts an overall fractionation from a super-chondritic Sm/Nd mantle composition to a TTG melt of around -0·13 Sm/Nd and -0·15 Lu/Hf, assuming 20% melting of a PUM mantle, 20% Isua basalt melting, and a Tp of 1540°C (Fig. 5). In isotopic terms, the fractionation from mantle to basalt for $^{147}Sm/^{144}Nd$ is -0·077 and for $^{176}Lu/^{177}Hf$ -0·021. This overall fractionation equates to an overall depletion from a mantle value of ∼300 ppb Nd and ∼42 ppb Hf. The super-chondritic Sm/Nd mantle composition (Sm/Nd = 0·373) represents an excess in Sm over a PUM composition of ∼60 ppb. We thus model an overall Nd depletion from mantle to TTG of the order of five times greater than the Nd enrichment required for the development of a super-chondritic Sm/Nd mantle.

Our modelling predicts that a chain of melting from a decoupled Hf–Nd mantle composition yields both basalt and TTG compositions that are also decoupled with respect to the Hf and Nd systems. This Hf–Nd isotopic fractionation trend from mantle through basalt to TTG is broadly parallel to, but offset from, those values which are isotopically coupled (Fig. 5), implying that a non-chondritic mantle composition may exert a major control in shifting the whole fractionation trend during melting away from isotopically coupled compositions in Hf–Nd space. These calculated decoupled Hf–Nd compositions, similar to those measured in Eoarchaean basalts and TTGs, will develop to lie off the εHf–εNd terrestrial array. Modelling a mantle of chondritic composition, in contrast, produces basaltic melt which diverges

from the Hf–Nd composition measured in the Isua basalts, and in turn generates melts of a TTG composition which are closer to having isotopically coupled values (Fig. 7a). Further, our modelling is relatively insensitive to changes in Tp, and degrees of mantle melting, as also shown in Fig. 7.

Signatures of crustal recycling and implications for isotopic decoupling

We suggest that the decoupled Hf–Nd isotopic compositions as measured in West Greenland Eoarchaean basalts and TTGs may reflect their extraction from a mantle which itself was isotopically decoupled. However, our modelling assumes that the mantle from which the basalts were extracted had not experienced any previous enrichment. Hoffmann et al. (2011b) invoked the presence of a light rare earth element (LREE)–enriched (metasomatic) component within the Isua mantle source. In this model, LREE elements would be preferentially liberated from a subducting slab as it devolatilized or melted (e.g. Kessel et al., 2005), thereby enriching the mantle reservoir in LREE, notably Nd (Jenner et al., 2009; Hoffmann et al., 2011b). This process would cause the mantle composition to evolve towards lower Sm/Nd values. LREE enrichment of a mantle source would also be expected to elevate its Lu/Hf composition. Notably, Eoarchaean metaboninites from Isua tend to have more radiogenic initial Hf isotope values above that of chondrite, in contrast to the tholeiitic melts considered here (Hoffmann et al., 2010), suggesting a more depleted mantle source.

Deviations are observed between the incompatible trace element ratios predicted by our model, and those measured in the Isua basalts (Fig. 6). The offsets are consistent with some degree of crustal contamination, the effects of which are illustrated by orange arrows in Fig. 6. This crustal contamination could either have occurred during magma chamber processes, or it could represent a mantle source overprint in the form of a melt-like subduction component, as proposed by Hoffmann et al. (2011b). Arguably, the elevated silica content of the Isua basalts (average here, ∼50 wt % SiO_2) may favour late-stage contamination within a magma chamber, because silica would likely have been buffered by olivine in the mantle (e.g. Yaxley & Green, 1998). However, it is hard to distinguish between these two crustal contamination scenarios on the basis of trace element compositions alone.

If the mantle source to the Isua basalts had been affected by crustal contamination, then as Fig. 6d highlights, this would have affected their Lu/Hf and Sm/Nd compositions or, conversely, basalts extracted from a pristine PUM mantle source (i.e. without crustal contamination) require higher degrees of mantle melting than previously inferred.

To further assess how a mantle contaminated with crustal material might affect the Hf–Nd composition of extracted basalts, we re-ran the modelling with a

modified mantle composition. For a continental crustal contaminant, we took an average composition of Itsaq Gneiss TTGs (n = 33; Nutman *et al.*, 2007; Hoffmann *et al.*, 2011*a*), which gives a modelled TTG contaminant with Lu/Hf = 0·029 and Sm/Nd = 0·126. We then created a "contaminated mantle" composition with 95% super-chondritic Sm/Nd PUM mantle and 5% of this average TTG contaminant. This contaminated mantle composition has Lu/Hf = 0·156 and Sm/Nd = 0·300 (red diamond, Fig. 9a). Also shown on Fig. 9a is the PUM melting path anchored at this contaminated mantle composition in $(Sm/Nd)_N$ vs $(Lu/Hf)_N$ space. The net effect of 5% TTG contaminant is that 30% mantle melting is required to produce melt with a composition similar to the Isua basalts (Fig. 9a).

Figure 9b shows how the originally super-chondritic Sm/Nd mantle composition varies in $(Sm/Nd)_N$ vs $(Lu/Hf)_N$ space as a function of degree of contamination (from 1% to 20%) by the average Itsaq Gneiss TTG. Beyond 5% contamination, the modelled mantle is more enriched than the average Isua basalts (red square, Fig. 9b), implying that at no degree of mantle melting could their Hf–Nd composition ever be attained. This puts an upper bound on the potential degree of crustal contamination that can be accommodated (i.e. it was ∼5% or less), at least within the bounds of our modelling.

Figure 7c shows the effect of 30% mantle melting (instead of 20%) on our overall chain of melting from mantle to TTG. This higher degree of mantle melting has the net effect of migrating the predicted Hf–Nd compositions of TTG melts towards more enriched Sm/Nd, and away from those measured in Itsaq Gneiss TTGs. Therefore, although higher degrees of contaminated mantle melting better accommodate the Isua basalt compositions, lower degrees of mantle melting better accommodate the ultimate TTG compositions. This contradiction may be explained by multi-generational melting, as discussed later.

Mantle Nd isotopic evolution

The Nd isotopic evolution of a mantle that developed a super-chondritic Sm/Nd composition in the early Hadean, and which persisted through to the Eoarchaean, determines the εNd of basalt extracted from it (i.e. initial $^{143}Nd/^{144}Nd$ normalized to CHUR). We assume a 4·47 Ga differentiation event to elevate the mantle composition to $^{147}Sm/^{144}Nd \sim 0\cdot221$ (Rizo *et al.*, 2011), which thereafter evolves and diverges from chondritic $^{143}Nd/^{144}Nd$ values (Fig. 10).
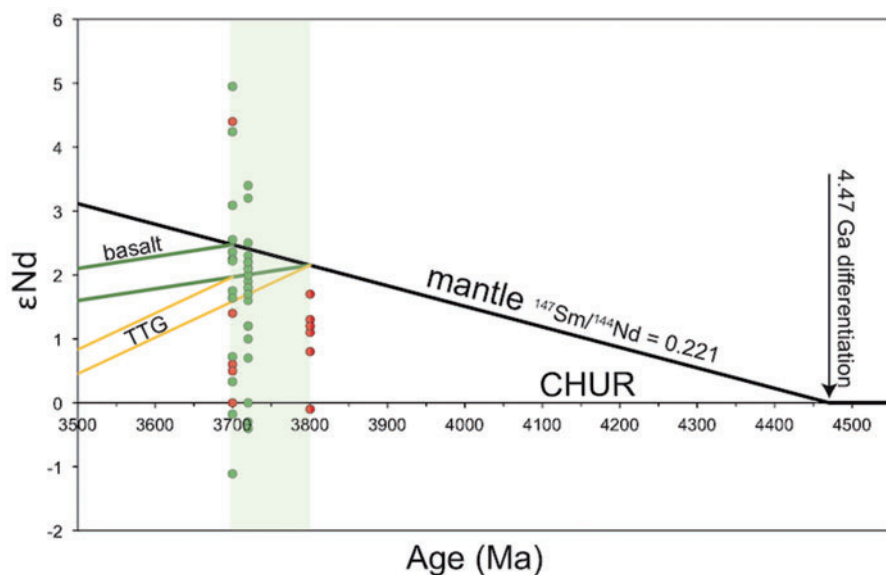
Extracting melt from this mantle composition at both 3·8 and 3·7 Ga yields basalts with an initial εNd_{3800} of +2·15 and εNd_{3700} +2·47, respectively. Although the data are scattered (Fig. 10), initial $^{143}Nd/^{144}Nd$ ratios measured in Eoarchaean Isua metabasalts are in general above that of CHUR and consistent with depletion of the mantle in Nd.
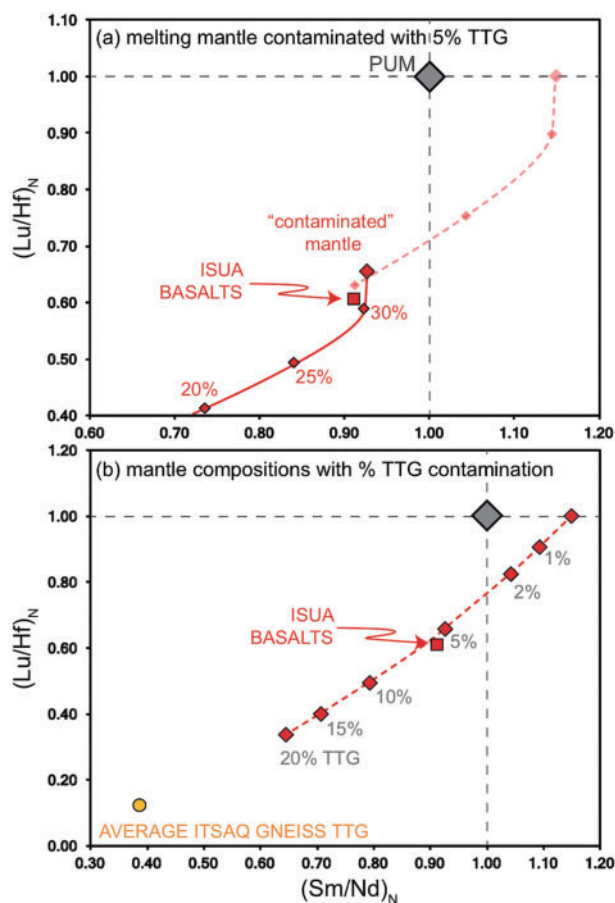
Fig. 9. (a) The effect of 5% crustal (TTG) contamination of a super-chondritic Sm/Nd mantle source, on the modelled basaltic melt. Axes are calculated Lu/Hf and Sm/Nd compositions normalized to PUM. The PUM melting curve is anchored at a modelled "contaminated mantle", comprising 5% average Itsaq Gneiss TTG and 95% super-chondritic Sm/Nd mantle (red diamond). Also plotted is the average Isua basalt $(Lu/Hf)_N$ and $(Sm/Nd)_N$ composition (red square). 30% melting of the contaminated mantle is required to produce a melt with a $(Lu/Hf)_N$ and $(Sm/Nd)_N$ composition similar to the Isua basalts. (b) The change in the $(Lu/Hf)_N$ and $(Sm/Nd)_N$ composition of a super-chondritic Sm/Nd mantle as a function of different degrees of TTG contamination (1–20%). Also plotted is the average Itsaq Gneiss TTG composition (orange circle). A modelled mantle composition with >5% TTG contaminant is more enriched than the Isua basalt (red square).

Hf–Nd melting arrays in the production of TTG

Garnet, which is predicted to be stable within the lower portions of thick plateau-like mafic crust and/or within down-going slabs at depth (e.g. Johnson *et al.*, 2017) may cause significant fractionation of Lu from Hf during basalt melting (Vervoort & Patchett, 1996; Gardiner *et al.*, 2018). Thus, deep melting of basalt may be one driver of Hf–Nd decoupling in Eoarchaean TTGs. Some leucosomes in the Isua basalts contain garnet, implying that melting occurred within the garnet stability field (Hoffmann *et al.*, 2014). The Isua basalts considered here are relatively Mg-rich, and for these our modelling calculates garnet only to be stable at pressures above ∼1·2 GPa, which compares well with the ∼1·1 GPa predicted by Hoffmann *et al.* (2019) for an Isua tholeiite

Fig. 10. Modelled Sm–Nd isotopic evolution of the Isua mantle reservoir and of extracted basalts and TTGs calculated as εNd. A mantle differentiation event at 4·47 Ga elevated the mantle $^{147}Sm/^{144}Nd$ to ~0·221 (model of Rizo *et al.*, 2011). Extracting melt from this mantle composition at both 3·8 and 3·7 Ga yields basalts with an initial εNd of +2·15 and +2·47, respectively. The basalt evolution trends are for $^{147}Sm/^{144}Nd = 0·1827$ calculated for 20% PUM melting, and the TTG evolution trends for $^{147}Sm/^{144}Nd = 0·153$, calculated for 20% Isua basalt melting. Calculations use the chondrite values of Bouvier *et al.* (2008), and the ^{147}Sm decay constant of Lugmair & Marti (1978). Also plotted are reported εNd from Isua metabasalts; red (Hoffmann *et al.*, 2011b); green (Blichert-Toft *et al.*, 1999, Hoffmann *et al.*, 2010).

using the same activity models. Thus, along the 900°C/GPa geothermal gradient, along which we model basalt melting, we do not predict garnet to be stable (Fig. 2). However, melt modelling the Isua basalts along cooler geotherms, i.e. at higher *P*, has garnet stable. Figure 7d shows the effect of melting the Isua basalts along a 700°C/GPa geothermal gradient, which includes the effect of restitic garnet (Fig. 2). Predicted TTG melt compositions for different degrees of melting are more clustered, but are not distinctly different to melting along the 900°C/GPa geothermal gradient (cf. Fig. 5).

Eoarchaean geodynamic settings

We estimate that 20–30% melting of the Eoarchaean mantle was required to produce basaltic melts with the Hf–Nd composition of the Isua metabasalts, depending on whether a crustal contaminant is taken into account. These inferred melt fractions compare well with the lower estimates (~15%) proposed to account for the Lu/Hf ratios of Archaean mafic crust calculated from Hf isotopes (Hawkesworth *et al.*, 2017). The estimates also match the range (20–30%) invoked for generation of primary (tholeiitic) basalts in the Archaean (Zegers & van Keken, 2001; Bédard, 2006; Herzberg *et al.*, 2010). However, our modelled melt fractions are slightly or much lower than those (25–45%) for Archaean tholeiitic basalts calculated from residual peridotites that sampled the Archaean lithospheric mantle (Herzberg & Rudnick, 2012).

Based on a modern mid-ocean ridge analogue, Herzberg & Rudnick (2012) proposed a simple

relationship by which ~1 km of primary crust results from ~1% mantle melting. If this relationship holds true for mantle melting in the Eoarchaean, ~20–30% melting equates to an original (i.e. unthickened) thickness for Eoarchaean primary crust in Isua of ~20–30 km. Estimates on the thickness of primitive crust in the Archaean vary from 20–35 km (Sleep & Windley, 1982; Abbott *et al.*, 1994; Ohta *et al.*, 1996), to in excess of 40 km (Herzberg & Rudnick, 2012). Non-uniformitarian models for the origin of Earth's first stable juvenile continental crust include the partial melting of hydrated basalts at the base of thickened oceanic plateaux (e.g. Smithies *et al.*, 2009; Johnson *et al.*, 2017). The volcanic plateau model for the origin of early felsic continental crust requires a minimum crustal thickness of the order of 30 km to induce melting at its base under assumed Archaean geothermal gradients (Johnson *et al.*, 2014). Our modelling has melting of the Isua basalts at depths of 35–45 km; melting at this depth implies significant crustal thickening (up to 150% or more) from our suggested original thickness of ~20–30 km. Similar to our predictions of 5–30 % basalt melting, other studies also propose ~20–30% basalt melting to produce early TTGs (e.g. Zegers & van Keken, 2001).

Production of primary basaltic crust in the early Earth required a significantly higher degree of mantle melting (~15–30%), possibly at greater depths, than at the present day. These factors point towards a distinct Hadean–Early Archaean geodynamic regime (Johnson *et al.*, 2017; O'Neil & Carlson, 2017), which is supported by the implied longevity (c. 500–1000 Ma) on the Earth's

surface of oceanic crust during the Hadean–Eoarchaean (Rizo *et al.*, 2012). Such longevity is consistent with the polycyclic reworking of basaltic crust invoked for some Archaean terranes, for example the East Pilbara Terrane, where current models have enriched non-tholeiitic basalts as parents to the juvenile Palaeoarchaean TTGs (Smithies *et al.*, 2009; Johnson *et al.*, 2017). These studies assume that the enriched basalts were themselves the product of melting more primitive basalt. A multi-stage melting history for the Isua tholeiitic basalts has also been proposed (Hoffmann *et al.*, 2014). Thus, the evolutionary chain of melting from mantle to TTG perhaps requires more additional steps than those modelled here (as implied earlier), the net effect of which will be to drive TTG compositions towards still more fractionated $f(^{176}Lu/^{177}Hf)$ and $f(^{147}Sm/^{144}Nd)$ values.

Secular mantle evolution

The observation that both basaltic and felsic Eoarchaean crustal rocks from West Greenland have decoupled $\varepsilon Hf–\varepsilon Nd$ compositions contrasts with Proterozoic and younger crustal rocks which define the terrestrial fractional array (Bennett *et al.*, 1993; Vervoort *et al.*, 2000; Hoffmann *et al.*, 2011*b*). In this contribution we postulate that decoupled Hf–Nd compositions measured in Eoarchaean crust may reflect their extraction from a non-chondritic mantle composition. Whether such a distinct mantle composition existed, or if so, whether it represented a global mantle signature, or was only a local phenomenon, is of debate. ^{142}Nd anomalies, implying a distinct mantle Sm/Nd composition, have also been measured in the Nuvvuagittuq Greenstone Belt, Canada (O'Neil *et al.*, 2008) although implications for mantle composition depend on whether these rocks are assigned Eoarchaean or Hadean ages (e.g. Rizo *et al.*, 2013). If a super-chondritic Sm/Nd mantle composition was indeed a global phenomenon during the Eoarchaean, then it implies that prior to the Proterozoic, perhaps as early as 3·4 Ga (Rizo *et al.*, 2012), the composition of the upper mantle returned to a coupled state, which may reflect re-homogenization through lower mantle melting and mixing. Earth's modern mantle is relatively well-mixed (Bina & Helffrich, 2014), driven by mantle convection and mass transfer through the mantle transition layer. A step-change in the efficacy of mantle mixing between the Hadean and Late Archaean may have been the result of enhanced plume activity (Maier *et al.*, 2009), or perhaps records the onset of global plate tectonics (O'Neill *et al.*, 2013), reflected in the isotopic composition of oceanic and continental crust extracted since at least the Early Proterozoic.

CONCLUSIONS

- Production of primary basaltic crust in the early Earth required a significantly higher degree of mantle melting (~20–30%) than present-day N-MORB, consistent with higher ambient mantle temperatures in the early Earth.
- Our modelling confirms that a modelled chain of melting from mantle though basalt to TTG defines an overall Hf–Nd isotopic fractionation trend that is parallel to that defined by modern rocks with coupled compositions. This is in line with expectations that the Lu/Hf and Sm/Nd systems behave in a similar manner during melting processes.
- Contamination of a mantle source with 5% recycled continental crustal (TTG) material means a higher degree of mantle melting (here, 30%) is required to produce basaltic melt that has a similar Hf–Nd composition to that generated from lower degrees of melting (20%) of an uncontaminated mantle. Modelling suggests >5% continental crustal contamination shifts mantle compositions to be more enriched than the average Isua basalts, thereby putting some upper limit on the amount of crustal contaminant.
- West Greenland Eoarchaean crustal rocks have decoupled Hf-Nd compositions that sit below the terrestrial fractionation trend, for which one model may be that they were extracted from a non-chondritic mantle source composition in the early Archaean.

APPENDIX

MELT PRODUCT TRACE ELEMENT COMPOSITIONS

Volume modes of mineral phases within the residuum are normalized to 100%. To estimate the elemental concentrations of trace elements in these melt products, a bulk partition coefficient (*D*) was calculated for each element from compiled phase-level distribution

coefficients (*Kd*) relevant to the melting of mafic and ultramafic rocks, using Equation A1, example for Hf, for *n* phases, where *X* is the mole fraction of phase *k*.

$$D_{bulk}^{Hf} = \sum_{k=0}^{n} K_k^{Hf}.X_k \qquad \text{(A1)}$$

Lu/Hf and Sm/Nd ratio calculation

The elemental Lu, Hf, Sm and Nd concentrations (*x*) were derived using Equation A2, where F is melt fraction and $x^{initial}$ is the concentration of the trace element in the parent, in this example Hf:

$$x_{Hf} = \frac{x_{Hf}^{initial}}{D_{bulk}^{Hf} + \left(F*\left(1 - D_{bulk}^{Hf}\right)\right)} \qquad \text{(A2)}$$

The calculated elemental Lu/Hf ratios in each melt product were then converted to isotopic ratios. The $^{176}Lu/^{177}Hf$ ratio can be calculated from whole-rock compositional data based on the atomic abundances (Meija *et al.*, 2016) and weights (de Laeter *et al.*, 2003) of the isotopes.

REFERENCES

Abbott, D., Drury, R. & Smith, W. H. F. (1994). Flat to steep transition in subduction style. *Geology* **22**, 937–940.

Allaart, J. H. (1976). The pre-3760 m.y. old supracrustal rocks of the Isua area, central West Greenland, and the associated occurrence of quartz-banded ironstone. In: Windley, B. F. (ed.) *The Early History of the Earth*. London: Wiley, pp. 177–189.

Bacon, C. R. & Druitt, T. H. (1988). Compositional evolution of the zoned calcalkaline magma chamber of Mount-Mazama, Crater Lake, Oregon. *Contributions to Mineralogy and Petrology* **98**, 224–256.

Bédard, J. H. (2006). A catalytic delamination-driven model for coupled genesis of Archaean crust and sub-continental lithospheric mantle. *Geochimica et Cosmochimica Acta* **70**, 1188–1214.

Bennett, V. C. (2003). Compositional evolution of the mantle. *Treatise on Geochemistry*. 2nd edn. pp. 493–519.

Bennett, V. C., Nutman, A. P. & McCulloch, M. T. (1993). Nd isotopic evidence for transient, highly depleted mantle reservoirs in the early history of the Earth. *Earth and Planetary Science Letters* **119**, 299–317.

Berry, A. J., Danyushevsky, L. V., St C. O'Neill, H., Newville, M. & Sutton, S. R. (2008). Oxidation state of iron in komatiitic melt inclusions indicates hot Archaean mantle. *Nature* **455**, 960–963.

Bézos, A. & Humler, E. (2005). The Fe3+/ΣFe ratios of MORB glasses and their implications for mantle melting. *Geochimica et Cosmochimica Acta* **69**, 711–725.

Bina, C. R. & Helffrich, G. (2014). Geophysical constraints on mantle composition. *Treatise on Geochemistry*. 2nd edn. pp. 41–65.

Blichert-Toft, J., Albarède, F., Rosing, M. T., Frei, R. & Bridgwater, D. (1999). The Nd and Hf isotopic evolution of the mantle through the Archean. Results from the Isua supracrustals, West Greenland, and from the Birimian terranes of West Africa. *Geochimica et Cosmochimica Acta* **63**, 3901–3914.

Boehnke, P., Watson, E. B., Trail, D., Harrison, T. M. & Schmitt, A. K. (2013). Zircon saturation re-revisited. *Chemical Geology* **351**, 324–334.

Bouvier, A., Vervoort, J. D. & Patchett, P. J. (2008). The Lu–Hf and Sm–Nd isotopic composition of CHUR: constraints from unequilibrated chondrites and implications for the bulk composition of terrestrial planets. *Earth and Planetary Science Letters* **273**, 48–57.

Boyet, M. & Carlson, R. (2006). A new geochemical model for the Earth's mantle inferred from 146Sm–142Nd systematics. *Earth and Planetary Science Letters* **250**, 254–268.

Boyet, M., Blichert-Toft, J., Rosing, M., Storey, M., Télouk, P. & Albarède, F. (2003). 142Nd evidence for early Earth differentiation. *Earth and Planetary Science Letters* **214**, 427–442.

Caro, G. & Bourdon, B. (2010). Non-chondritic Sm/Nd ratio in the terrestrial planets: consequences for the geochemical evolution of the mantle–crust system. *Geochimica et Cosmochimica Acta* **74**, 3333–3349.

Caro, G., Bourdon, B., Birck, J.-L. & Moorbath, S. (2006). High-precision 142Nd/144Nd measurements in terrestrial rocks: constraints on the early differentiation of the Earth's mantle. *Geochimica et Cosmochimica Acta* **70**, 164–191.

Caro, G., Bourdon, B., Wood, B. J. & Corgne, A. (2005). Trace-element fractionation in Hadean mantle generated by melt segregation from a magma ocean. *Nature* **436**, 246–249.

Chauvel, C., Lewin, E., Carpentier, M., Arndt, N. T. & Marini, J.-C. (2008). Role of recycled oceanic basalt and sediment in generating the Hf–Nd mantle array. *Nature Geoscience* **1**, 64–67.

Corgne, A., Liebske, C., Wood, B. J., Rubie, D. C. & Frost, D. J. (2005). Silicate perovskite-melt partitioning of trace elements and geochemical signature of a deep perovskitic reservoir. *Geochimica et Cosmochimica Acta* **69**, 485–496.

de Laeter, J. R., Bohlke, J. K., De Bievre, P., Hidaka, H., Peiser, H. S., Rosman, K. J. R. & Taylor, P. D. P. (2003). Atomic weights of the elements: review 2000. *Pure and Applied Chemistry* **75**, 683–800.

Dhuime, B., Hawkesworth, C., Cawood, P. A. & Storey, C. D. (2012). A change in the geodynamics of continental growth 3 billion years ago. *Science* **335**, 1334–1336.

Drummond, M. S. & Defant, M. J. (1990). A model for Trondhjemite-Tonalite-Dacite Genesis and crustal growth via slab melting: Archean to modern comparisons. *Journal of Geophysical Research* **95**, 21503.

Elkins, L., Gaetani, G. & Sims, K. (2008). Partitioning of U and Th during garnet pyroxenite partial melting: constraints on the source of alkaline ocean island basalts. *Earth and Planetary Science Letters* **265**, 270–286.

Fisher, C. M. & Vervoort, J. D. (2018). Using the magmatic record to constrain the growth of continental crust—the Eoarchean zircon Hf record of Greenland. *Earth and Planetary Science Letters* **488**, 79–91.

Gardiner, N. J., Johnson, T. E., Kirkland, C. L. & Smithies, R. H. (2018). Melting controls on the lutetium–hafnium evolution of Archaean crust. *Precambrian Research* **305**, 479–488.

Green, E. C. R., White, R. W., Diener, J. F. A., Powell, R., Holland, T. J. B. & Palin, R. M. (2016). Activity-composition relations for the calculation of partial melting equilibria in metabasic rocks. *Journal of Metamorphic Geology* **34**, 845–869.

Harui, E. H., Wagner, T. P. & Grove, T. L. (1994). Experimental and natural partitioning of Th, U, Pb and other trace elements between garnet, clinopyroxene and basaltic melts. *Chemical Geology* **117**, 149–166.

Hawkesworth, C., Cawood, P. A., Dhuime, B. & Kemp, A. I. (2017). Earth's continental lithosphere through time. *Annual Review of Earth and Planetary Sciences* **45**, 169–198.

Herzberg, C. & Rudnick, R. (2012). Formation of cratonic lithosphere: an integrated thermal and petrological model. *Lithos* **149**, 4–15.

Herzberg, C., Condie, K. & Korenaga, J. (2010). Thermal history of the Earth and its petrological expression. *Earth and Planetary Science Letters* **292**, 79–88.

Hiess, J. & Bennett, V. C. (2016). Chondritic Lu/Hf in the early crust–mantle system as recorded by zircon populations from the oldest Eoarchean rocks of Yilgarn Craton, West Australia and Enderby Land, Antarctica. *Chemical Geology* **427**, 125–143.

Hiess, J., Bennett, V. C., Nutman, A. P. & Williams, I. S. (2009). In situ U–Pb, O and Hf isotopic compositions of zircon and olivine from Eoarchaean rocks, West Greenland: new insights to making old crust. *Geochimica et Cosmochimica Acta* **73**, 4489–4516.

Hoffmann, J. E., Münker, C., Næraa, T., Rosing, M. T., Herwartz, D., Garbe-Schönberg, D. & Svahnberg, H. (2011). Mechanisms of Archean crust formation inferred from high-precision HFSE systematics in TTGs. *Geochimica et Cosmochimica Acta* **75**, 4157–4178.

Hoffmann, J. E., Münker, C., Polat, A., König, S., Mezger, K. & Rosing, M. T. (2010). Highly depleted Hadean mantle reservoirs in the sources of early Archean arc-like rocks, Isua supracrustal belt, southern West Greenland. *Geochimica et Cosmochimica Acta* **74**, 7236–7260.

Hoffmann, J. E., Münker, C., Polat, A., Rosing, M. T. & Schulz, T. (2011). The origin of decoupled Hf–Nd isotope compositions in Eoarchean rocks from southern West Greenland. *Geochimica et Cosmochimica Acta* **75**, 6610–6628.

Hoffmann, J. E., Nagel, T. J., Münker, C., Næraa, T. & Rosing, M. T. (2014). Constraining the process of Eoarchean TTG formation in the Itsaq Gneiss Complex, southern West Greenland. *Earth and Planetary Science Letters* **388**, 374–386.

Hoffmann, J. E., Zhang, C., Moyen, J.-F. & Nagel, T. J. (2019). The formation of Tonalites–Trondjhemite–Granodiorites in Early continental crust. In: Van Kranendonk, M. J., Bennett, V. C. and Hoffmann, J. E. (eds) *Earth's Oldest Rocks*. Amsterdam: Elsevier, pp. 133–168.

Hofmann, A. W. (1988). Chemical differentiation of the Earth: the relationship between mantle, continental crust, and oceanic crust. *Earth and Planetary Science Letters* **90**, 297–314.

Holland, T. J. B. & Powell, R. (2003). Activity–composition relations for phases in petrological calculations: an asymmetric multicomponent formulation. *Contributions to Mineralogy and Petrology* **145**, 492–501.

Holland, T. J. B. & Powell, R. (2011). An improved and extended internally consistent thermodynamic dataset for phases of petrological interest, involving a new equation of state for solids. *Journal of Metamorphic Geology* **29**, 333–383.

Holland, T. J. B., Green, E. C. R. & Powell, R. (2018). Melting of Peridotites through to granites: a simple thermodynamic model in the system KNCFMASHTOCr. *Journal of Petrology* **59**, 881–900.

Irving, A. J. & Frey, F. A. (1976). Effect of composition on partitioning of rare-earth elements, Hf, Sc and Co between garnet and liquid—experimental and natural evidence. *EOS, Transactions of the American Geophysical Union* **57**, 339–339.

Jackson, C. R. M., Ziegler, L. B., Zhang, H., Jackson, M. G. & Stegman, D. R. (2014). A geochemical evaluation of potential magma ocean dynamics using a parameterized model for perovskite crystallization. *Earth and Planetary Science Letters* **392**, 154–165.

Jenner, F. E., Bennett, V. C., Nutman, A. P., Friend, C. R. L., Norman, M. & Yaxley, G. (2009). Evidence for subduction at 3.8 Ga: geochemistry of arc-like metabasalts from the southern edge of the Isua Supracrustal Belt. *Chemical Geology* **261**, 83–98.

Jennings, E. S. & Holland, T. J. B. (2015). A simple thermodynamic model for melting of peridotite in the system NCFMASOCr. *Journal of Petrology* **56**, 869–892.

Johnson, T. E., Brown, M., Gardiner, N. J., Kirkland, C. L. & Smithies, R. H. (2017). Earth's first stable continents did not form by subduction. *Nature* **543**, 239–242.

Johnson, T. E., Brown, M., Kaus, B. J. P. & VanTongeren, J. A. (2014). Delamination and recycling of Archaean crust caused by gravitational instabilities. *Nature Geoscience* **7**, 47–52.

Katsura, T., Yoneda, A., Yamazaki, D., Yoshino, T. & Ito, E. (2010). Adiabatic temperature profile in the mantle. *Physics of the Earth and Planetary Interiors* **183**, 212–218.

Kennedy, A. K., Lofgren, G. E. & Wasserburg, G. J. (1993). An experimental-study of trace-element partitioning between olivine, ortho-pyroxene and melt in chondrules - equilibrium values and kinetic effects. *Earth and Planetary Science Letters* **115**, 177–195.

Kessel, R., Schmidt, M. W., Ulmer, P. & Pettke, T. (2005). Trace element signature of subduction-zone fluids, melts and supercritical liquids at 120-180 km depth. *Nature* **437**, 724–727.

Labrosse, S., Hernlund, J. W. & Coltice, N. (2007). A crystallizing dense magma ocean at the base of the Earth's mantle. *Nature* **450**, 866–869.

Liebske, C., Corgne, A., Frost, D. J., Rubie, D. C. & Wood, B. J. (2005). Compositional effects on element partitioning between Mg-silicate perovskite and silicate melts. *Contributions to Mineralogy and Petrology* **149**, 113–128.

Lugmair, G. W. & Marti, K. (1978). Lunar initial 143Nd/144Nd: differential evolution of the lunar crust and mantle. *Earth and Planetary Science Letters* **39**, 349–357.

Maier, W. D., Barnes, S. J., Campbell, I. H., Fiorentini, M. L., Peltonen, P., Barnes, S.-J. & Smithies, R. H. (2009). Progressive mixing of meteoritic veneer into the early Earth's deep mantle. *Nature* **460**, 620–623.

Martin, H. (1994). The Archean grey gneisses and the genesis of continental crust. *Developments in Precambrian Geology* **11**, 205–259.

McDonough, W. F. & Sun, S. S. (1995). The composition of the Earth. *Chemical Geology* **120**, 223–253.

McKenzie, D. & Bickle, M. J. (1988). The volume and composition of melt generated by extension of the lithosphere. *Journal of Petrology* **29**, 625–679.

McKenzie, D. & O'Nions, R. K. (1991). Partial melt distributions from inversion of rare earth element concentrations. *Journal of Petrology* **32**, 1021–1091.

Meija, J., Coplen, T. B., Berglund, M., Brand, W. A., De Bievre, P., Groning, M., Holden, N. E., Irrgeher, J., Loss, R. D., Walczyk, T. & Prohaska, T. (2016). Isotopic compositions of the elements 2013 (IUPAC Technical Report). *Pure Applied Chemistry* **88**, 293–306.

Moorbath, S., Whitehouse, M. & Kamber, B. S. (1997). Extreme Nd-isotope heterogeneity in the early Archaean—fact or fiction? Case histories from northern Canada and West Greenland. *Chemical Geology* **135**, 213–231.

Morino, P., Caro, G., Reisberg, L. & Schumacher, A. (2017). Chemical stratification in the post-magma ocean Earth

inferred from coupled 146, 147 Sm–142, 143 Nd systematics in ultramafic rocks of the Saglek block (3.25–3.9 Ga; northern Labrador, Canada). *Earth and Planetary Science Letters* **463**, 136–150.

Moyen, J.-F. (2011). The composite Archaean grey gneisses: petrological significance, and evidence for a non-unique tectonic setting for Archaean crustal growth. *Lithos* **123**, 21–36.

Næraa, T., Scherstén, A., Rosing, M. T., Kemp, A. I. S., Hoffmann, J. E., Kokfelt, T. F. & Whitehouse, M. J. (2012). Hafnium isotope evidence for a transition in the dynamics of continental growth 3.2 Gyr ago. *Nature* **485**, 627–630.

Nagel, T. J., Hoffmann, J. E. & Munker, C. (2012). Generation of Eoarchean tonalite-trondhjemite-granodiorite series from thickened mafic arc crust. *Geology* **40**, 375–378.

Nutman, A., McGregor, V. R., Friend, C. L., Bennett, V. C. & Kinny, P. D. (1996). The Itsaq Gneiss Complex of southern West Greenland; the world's most extensive record of early crustal evolution (3900-3600 Ma). *Precambrian Research* **78**, 1–39.

Nutman, A. P., Bennett, V. C., Friend, C. R. L., Horie, K. & Hidaka, H. (2007). ∼3,850 Ma tonalites in the Nuuk region, Greenland: geochemistry and their reworking within an Eoarchaean gneiss complex. *Contributions to Mineralogy and Petrology* **154**, 385–408.

Nutman, A. P., Bennett, V. C., Friend, C. R. L. & Norman, M. (1999). Meta-igneous (non-gneissic) tonalites and quartz-diorites from an extensive ca. 3800 Ma terrain south of the Isua supracrustal belt, southern West Greenland: constraints on early crust formation. *Contributions to Mineralogy and Petrology* **137**, 364–388.

O'Neil, J. & Carlson, R. W. (2017). Building Archean cratons from Hadean mafic crust. *Science* **355**, 1199–1202.

O'Neil, J., Carlson, R. W., Francis, D. & Stevenson, R. (2008). Neodymium-142 Evidence for Hadean Mafic Crust. *Science* **321**, 1828–1831.

O'Neill, C., Debaille, V. & Griffin, W. (2013). Deep Earth recycling in the Hadean and constraints on surface tectonics. *American Journal of Science* **313**, 912–932.

Ohta, H., Maruyama, S., Takahashi, E., Watanabe, Y. & Kato, Y. (1996). Field occurrence, geochemistry and petrogenesis of the Archean Mid-Oceanic Ridge Basalts (AMORBs) of the Cleaverville area, Pilbara Craton, Western Australia. *Lithos* **37**, 199–221.

Palme, H., Lodders, K. & Jones, A. (2014). Solar system abundances of the elements. *Treatise on Geochemistry*, 2nd edn. pp. 15–36.

Patchett, P. J. & Tatsumoto, M. (1980). Hafnium isotope variations in oceanic basalts. *Geophysical Research Letters* **7**, 1077–1080.

Plank, T., Spiegelman, M., Langmuir, C. H. & Forsyth, D. W. (1995). The meaning of "meanF": clarifying the mean extent of melting at ocean ridges. *Journal of Geophysical Research: Solid Earth* **100**, 15045–15052.

Polat, A. & Hofmann, A. W. (2003). Alteration and geochemical patterns in the 3.7–3.8 Ga Isua greenstone belt, West Greenland. *Precambrian Research* **126**, 197–218.

Polat, A., Hofmann, A. W., Munker, C., Regelous, M. & Appel, P. W. U. (2003). Contrasting geochemical patterns in the 3.7–3.8 Ga pillow basalt cores and rims, Isua greenstone belt, Southwest Greenland: implications for postmagmatic alteration processes. *Geochimica et Cosmochimica Acta* **67**, 441–457.

Powell, R. & Holland, T. J. B. (1988). An internally consistent dataset with uncertainties and correlations: 3. Applications to geobarometry, worked examples and a computer program. *Journal of Metamorphic Geology* **6**, 173–204.

Rizo, H., Boyet, M., Blichert-Toft, J., O'Neil, J., Rosing, M. T. & Paquette, J.-L. (2012). The elusive Hadean enriched reservoir revealed by 142Nd deficits in Isua Archaean rocks. *Nature* **491**, 96–100.

Rizo, H., Boyet, M., Blichert-Toft, J. & Rosing, M. (2011). Combined Nd and Hf isotope evidence for deep-seated source of Isua lavas. *Earth and Planetary Science Letters* **312**, 267–279.

Rizo, H., Boyet, M., Blichert-Toft, J. & Rosing, M. T. (2013). Early mantle dynamics inferred from 142Nd variations in Archean rocks from southwest Greenland. *Earth and Planetary Science Letters* **377–378**, 324–335.

Sawyer, E. W., Cesare, B. & Brown, M. (2007). When the continental crust melts. *Elements* **7**, 229–234.

Schmitz, M. D., Vervoort, J. D., Bowring, S. A. & Patchett, P. J. (2004). Decoupling of the Lu-Hf and Sm-Nd isotope systems during the evolution of granulitic lower crust beneath southern Africa. *Geology* **32**, 405.

Shaw, D. M. (1979). Trace element melting models. *Physics and Chemistry of the Earth* **11**, 577–586.

Sleep, N. H. & Windley, B. F. (1982). Archean plate tectonics: constraints and inferences. *The Journal of Geology* **90**, 363–379.

Smithies, R. H., Champion, D. C. & Van Kranendonk, M. J. (2009). Formation of Paleoarchean continental crust through infracrustal melting of enriched basalt. *Earth and Planetary Science Letters* **281**, 298–306.

Sun, S. S. & McDonough, W. F. (1989). Chemical and isotopic systematics of oceanic basalts: implications for mantle composition and processes. *Geological Society, London, Special Publications* **42**, 313–345.

Szilas, K., Kelemen, P. B. & Rosing, M. T. (2015). The petrogenesis of ultramafic rocks in the >3.7Ga Isua supracrustal belt, southern West Greenland: geochemical evidence for two distinct magmatic cumulate trends. *Gondwana Research* **28**, 565–580.

Vervoort, J. D. & Patchett, P. J. (1996). Behavior of hafnium and neodymium isotopes in the crust: constraints from Precambrian crustally derived granites. *Geochimica et Cosmochimica Acta* **60**, 3717–3733.

Vervoort, J. D., Patchett, P. J., Albarède, F., Blichert-Toft, J., Rudnick, R. L. & Downes, H. (2000). Hf-Nd isotopic evolution of the lower crust. *Earth and Planetary Science Letters* **181**, 115–129.

Vervoort, J. D., Patchett, P. J., Blichert-Toft, J. & Albarède, F. (1999). Relationships between Lu–Hf and Sm–Nd isotopic systems in the global sedimentary system. *Earth and Planetary Science Letters* **168**, 79–99.

Vervoort, J. D., Patchett, P. J., Gehrels, G. E. & Nutman, A. P. (1996). Constraints on early Earth differentiation from hafnium and neodynium isotopes. *Nature* **379**, 624–627.

White, R. W., Powell, R. & Clarke, G. L. (2002). The interpretation of reaction textures in Fe- rich metapelitic granulites of the Musgrave Block, Central Australia: constraints from mineral equilibria calculations in the system. *Journal of Metamorphic Geology* **20**, 41–55.

White, R. W., Powell, R., Holland, T. J. B., Johnson, T. E. & Green, E. C. R. (2014). New mineral activity-composition relations for thermodynamic calculations in metapelitic systems. *Journal of Metamorphic Geology* **32**, 261–286.

White, R. W., Powell, R., Holland, T. J. B. & Worley, B. A. (2000). The effect of TiO2 and Fe2O3 on metapelitic assemblages at greenschist and amphibolite facies conditions: mineral equilibria calculations in the system K2O–FeO–MgO–Al2O3–SiO2–H2O–TiO2–Fe2O3. *Journal of Metamorphic Geology* **18**, 497–511.

Workman, R. K. & Hart, S. R. (2005). Major and trace element composition of the depleted MORB mantle (DMM). *Earth and Planetary Science Letters* **231**, 53–72.

Yaxley, G. M. & Green, D. H. (1998). Reactions between eclogite and peridotite: mantle refertilisation by subduction of oceanic crust. *Schweizerische Mineralogische Und Petrographische Mitteilungen* **78**, 243–255.

Zegers, T. E. & van Keken, P. E. (2001). Middle Archean continent formation by crustal delamination. *Geology* **29**, 1083–1086.

Zhu, W., Gaetani, G., Fusseis, F., Montési, L. G. J. & De Carlo, F. (2011). Microtomography of partially molten rocks: three-dimensional melt distribution in mantle peridotite. *Science* **332**, 88–91.